Precambrian Research 275 (2016) 18–34

Contents lists available at ScienceDirect

Precambrian Research

journal homepage: www.elsevier.com/locate/precamres

Growth and evolution of Precambrian continental crust in the southwestern Tarim terrane: New evidence from the ca. 1.4 Ga A-type granites and Paleoproterozoic intrusive complex

Xian-Tao Ye[a,b], Chuan-Lin Zhang[b,*], M. Santosh[c,d], Jian Zhang[e], Xian-Ke Fan[b], Ji-Jun Zhang[f]

[a] Chinese Academy of Geological Sciences, Beijing 100037, China
[b] Nanjing Institute of Geology and Mineral Resources, Nanjing 210016, China
[c] Centre for Tectonics, Resources and Exploration, School of Physical Sciences, University of Adelaide, Adelaide, SA 5005, Australia
[d] School of Earth Sciences and Resources, China University of Geosciences Beijing, 29 Xueyuan Road, Beijing 100083, China
[e] Tianjin Institute of Geology and Mineral Resources, Tianjin 300170, China
[f] Shaanxi Center of Geological Survey, Xi'an 710068, China

ARTICLE INFO

Article history:
Received 19 August 2015
Received in revised form
21 November 2015
Accepted 27 December 2015
Available online 2 January 2016

Keywords:
Zircon geochronology
Nd–Hf–O isotopes
Geochemistry
Crustal growth
Tarim Craton

ABSTRACT

The Precambrian tectonic evolution and growth of continental crust in the southwestern Tarim Craton in NW China remain enigmatic. In this contribution, we report petrography, zircon U–Pb ages, geochemistry and Nd–Hf–O isotope data on the ca. 1.4 Ga granitic pluton in southwestern Tarim Terrane. We also present zircon U–Pb ages and Hf isotope data on the Paleoproterozoic intrusive complex from this area, and use the combined data to evaluate Precambrian tectonic evolution of the region in relation to the Columbia supercontinent. The ca. 1.4 Ga Azibailedi pluton is mainly composed of biotite monzogranite with contents SiO_2 (72.8–75.1 wt.%). The major element chemistry of the pluton reveals alkali-calcic and ferroan affinities and metaluminous to peraluminous feature with A/CNK ranging from 0.86 to 1.15. The granite shows high total REE contents with variable enrichment in LREE ($(La/Yb)_N$ = 8.5–12.2). Both REE and other incompatible elements features define A-type affinities. The initial epsilon Nd values vary from −3.5 to −2.2 and zircon $\varepsilon_{Hf}(t)$ and $\delta^{18}O$ values range from −4.1 to +6.1 and 7.1‰ to 8.6‰. Integrating geological, geochemical and Nd–Hf–O isotope data, we suggest that the Azibailedi A-type granites were derived from pre-existing early Paleoproterozoic mafic lower crust with involvement of variable amount of Paleoproterozoic juvenile crust, possibly trigged by basaltic magma upwelling, during the breakup of the Columbia supercontinent.

U–Pb geochronology and Hf isotopic analyses of zircons from the Paleoproterozoic Heluositan intrusive complex show crustal growth episodes during 2.2–4.2 Ga with peaks at 2.3–2.5 Ga, 3.3 Ga and 3.6–3.8 Ga, distinct from the other Precambrian terranes of the Tarim Craton. A comprehensive synthesis of the records of assembly and breakup of Columbia supercontinent from different Precambrian terranes in the Tarim Craton show significant differences. The temporal distinction in tectonothermal events and the marked difference in the continental crust growth processes suggest that the early Precambrian basement of the Tarim Craton was possibly composed of discrete terranes which were fragmented from different ancient cratonic nuclei.

1. Introduction

The Tarim, North China and South China Cratons constitute the three major Precambrian cratons in China (Zhao and Cawood, 2012; Zhang et al., 2013a,b). The Tarim Craton is located within the Xinjiang Uygur Autonomous Region of NW China, and is largely covered by desert (more than 85%) (Xu et al., 2013). The Precambrian basement rocks in the craton are exposed only along its margins, including the Tikelike area in the southwestern margin, the Akesu and Quruqtagh (also spelled as Kuluketage) area along the northern margin, and the North Altyn Tagh Mountain and the Dunhuang area at the eastern margin (Fig. 1a).

Investigations focusing on the Neoproterozoic geology of the southwestern Tarim terrane have revealed two tectonothermal episodes, one during early Neoproterozoic (1.0–0.9 Ga) and the other during middle Neoproterozoic (~0.8 Ga), possibly

* Corresponding author. Tel.: +86 25 84897863; fax: +86 25 84600446.
E-mail address: zchuanlin1968@gmail.com (C.-L. Zhang).

http://dx.doi.org/10.1016/j.precamres.2015.12.017
0301-9268/

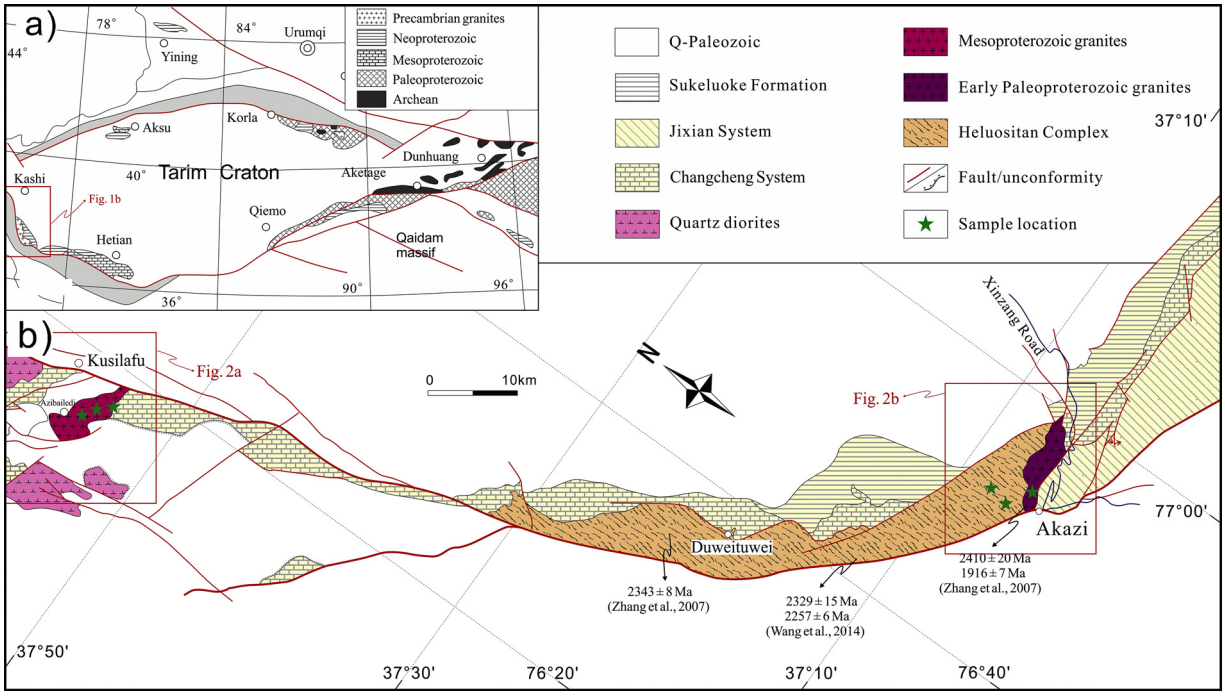

Fig. 1. (a) Tectonic framework of the Tarim Craton and its marginal area showing the Precambrian terranes along its margin. (b) Precambrian geology in the southwestern section of the Tarim Craton (modified after HNGS, 2004a,b).

corresponding to the assembly and breakup of the supercontinent Rodinia (Zhang et al., 2006a,b, 2010). However, despite the availability of some geochronological and geochemical data have been reported (Wang et al., 2014; Zhang et al., 2007a), continental growth processes and tectonic evolution are poorly understood.

In this contribution, we present detailed field observations, petrography, zircon U–Pb ages and Hf–O isotopes, whole-rock major and trace element geochemistry, and Sr–Nd isotopes of the Azibailedi A-type granites (ferroan granites) in the southwestern margin of Tarim Craton. We also report zircon U–Pb ages and Hf isotopes of the early Paleoproterozoic Heluositan intrusive complex, which findings, in combination with those from previous investigations provide new insights into: (1) the petrogenesis of the 1.4 Ga Azibailedi A-type granites, and their implications on the history of breakup of the Columbia supercontinent; (2) the Precambrian tectonic evolution and continental crustal growth and (3) the architecture of the early Precambrian basement of the Tarim Craton.

2. Regional geology

The Tarim Craton is bound by the Tianshan, Western Kunlun and Central-Southern Altyn-Tagh mountain belts to the north, south and southeast, respectively (Fig. 1a) (Lu et al., 2008; Zhang et al., 2013a). The craton shows typical double-layered structure consisting of a Precambrian basement (pre-Neoproterozoic) and late Neoproterozoic to Cambrian cover series (Xinjiang BGMR, 1993; Feng et al., 1995). The Precambrian rocks in the Tarim Craton are mostly exposed along the northern, eastern and southwestern margins.

The Precambrian basement rocks of the Quruqtagh-Dunhuang area are composed of orthogneisses (tonalite-trondhjemite-granodiorite; TTG), amphibolite and metasedimentary rocks. Previous studies indicated that the TTG rocks were mainly emplaced at ca. 2.7–2.5 Ga. Metamorphism main at ca. 1.85–1.80 Ga has been identified in both Archean and the Paleoproterozoic paragneisses (Ge et al., 2014; Zhang et al., 2013b) and the Paleoproterozoic metamorphism has been correlated to the assembly of the Columbia supercontinent (Ge et al., 2013a; Zhang et al., 2012a, 2013b; Lei et al., 2012). A recent study on 1470 Ma metadiabase from this region correlates with the breakup of the Columbia supercontinent (Wu et al., 2014). In the Aketage area, Paleoproterozoic metamorphic events are recorded by the Archean Milan Group, mostly composed of TTG rocks, hypersthene granulite, and mafic granulite, metamorphosed at ~2.0 Ga (Zhang et al., 2014a), followed by 1.85 Ga post-orogenic extension represented by OIB-like mafic dykes and massive potassic granites (Lu et al., 2008; Zhang et al., 2014a). Detrital zircon U–Pb dating and field mapping indicate the absence of Archean basement in the Akesu area (Fig. 1a) (Xinjiang BGMR, 1993; Zhang et al., 2014b). Zircons from the Akesu Group have U–Pb age populations of ~0.82 Ga, 2.0–1.8 Ga, ~2.3 Ga and ~2.5 Ga (Zhang et al., 2014b; Zhu et al., 2011). The youngest group of these ages at ~820 Ma constrains the lower limit of the depositional time of the protoliths of Aksu blueschist (Zhang et al., 2014b). The age population of 2.0–1.8 Ga is coincident with the timing of the amalgamation of the Columbia supercontinent (Zhu et al., 2011). Based on zircon U–Pb ages and $^{39}Ar/^{40}Ar$ plateau age of glaucophane from the blueschist in Aksu terrane (Yong et al., 2013), Zhang et al. (2014a,b) argued that the Akesu terrane (AT) might represent an accretionary terrane amalgamated to the Tarim Craton during 820–780 Ma.

The major Precambrian units of the southwestern Tarim terrane (STT) are mainly composed of the Paleoproterozoic Heluositan complex, the Mesoproterozoic greenschist-facies metamorphosed and intensively folded sedimentary sequences and the Neoproterozoic volcanic-sedimentary sequences with no significant metamorphism and deformation (Zhang et al., 2007a,b, 2010) (Fig. 1b). The Heluositan Complex mainly consists of paragneisses, orthogneisses and migmatites which underwent ca. 1.9 Ga amphibolite to granulite facies metamorphism and were intruded by the 2.34 Ga Xuxugou and 2.41 Ga Akazi plutons (Zhang et al., 2007a; Guo et al., 2013). Furthermore, the ca. 1.9 Ga metamorphism event has also been recorded in the complex (Wang et al., 2014; Zhang et al., 2007a). The poorly exposed Mesoproterozoic magmatic rocks occur in the northern part of the Tikelike belt close to Kusilafu area

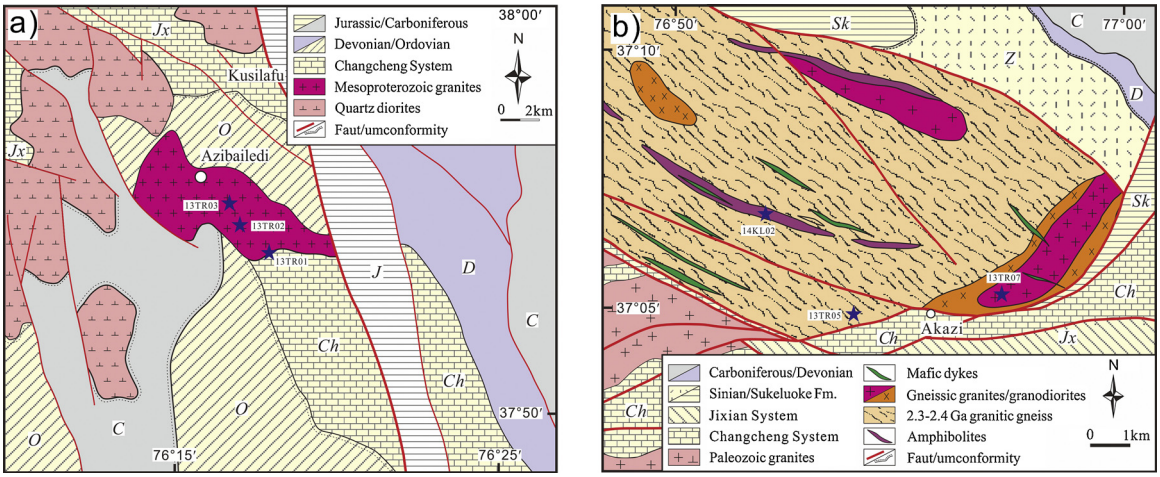

Fig. 2. (a) Geological map of the Azibailedi pluton. (b) Geological map of the Akazi pluton and amphibolites from the Heluositan Complex. The number and the star symbol show the sample number and the sampling locality.

of the Aketao County (Fig. 2a). These rocks were first reported in the STT by Huang et al. (2012). However, their petrogenesis and tectonics need further discussion.

3. Petrography

3.1. Azibailedi A-type granites

The Azibailedi pluton is located in the north-western section of the STT (Fig. 1b) with an outcrop area covering 12 km^2. The pluton intruded Mesoproterozoic carbonate rocks of the Changcheng system. The Changcheng system was unconformably covered by Ordovician-Carboniferous sandstone and conglomerate (Fig. 2a). Migmatite developed along the margin of the Azibailedi pluton. The Changcheng System carbonate rocks were extensively invaded by high temperature granitic melts, and therefore the zircon growth in the migmatite and granite occurred coevally. The migmatite shows banded structure and is mainly comprised quartz and feldspar phenocrysts set within a felsic matrix with minor carbonate minerals (Fig. 3a and g). The Azibailedi pluton is relatively homogeneous with the main rock type being biotite monzogranite. The rock shows grayish color and of gneissic structure (Fig. 3b and c), with medium to coarse granitic texture. The mineralogy is defined by K-feldspar (30–45%), plagioclase (25–35%), quartz (25–30%), biotite (5–7%), hornblende (less than 2%) with accessory minerals such as zircon, titanite and monazite (Fig. 3h). Recrystallized quartz and biotite suggest metamorphism and/or deformation after emplacement (Fig. 3i).

3.2. The granitic rocks and amphibolites from Heluositan Complex

The petrography of Akazi pluton has been described in detail by Zhang et al. (2007a) and Wang et al. (2014). The main rock types are pinkish granodiorite and quartz monzonite (Fig. 2b) showing medium to coarse texture and gneissic structure. The presence of remelting textures indicates that the rocks witnessed post-emplacement metamorphism, as is also evident from the core-rim structure of the zircons grains from this pluton (Zhang et al., 2007a).

The gneissic granites are quartz monzonite (Fig. 2b) which display medium to coarse-grained texture and strong gneissic structure (Fig. 3d–f). The dominant minerals are plagioclase (30–40%), K-feldspar (25–35%), Quartz (25–30%), biotite (5–7%), hornblende (2–5%) together with accessory minerals such as apatite and zircon.

An amphibolite dyke of about 3 km in length and 200–300 m width intrudes the Heluositan granitic gneiss (Fig. 2b). The rock is medium to coarse grained, dark in color and shows gneissic structure. It is dominantly composed of hornblende (50–60%), plagioclase (30–40%), biotite (2–5%) and minor pyroxene (1–2%) (Fig. 3j–l). Apatite and Ti–Fe oxide occur as accessory minerals. The mineral assemblage suggests mafic protolith.

4. Analytical methods

Zircon separation was carried out using conventional heavy liquid and magnetic techniques. Zircon grains and zircon standards were then hand-picked under a binocular microscope and representative grains and zircon standards were mounted in an epoxy resin disk, and then polished to about half their thickness. Zircons were photographed under transmitted and reflected light and their cathodoluminescence (CL) images to reveal their internal structures.

Zircon U–Pb analyses were carried out using LA-ICP-MS techniques at Tianjin Institute of Geology and Mineral Resources. The detailed analytical procedures were after Geng et al. (2011) and Hou et al. (2009). Data reduction was performed off-line by ICPMS-DataCal (Liu et al., 2009, 2010) and ISOPLOT (Ludwig, 1999). The weighted mean ages are quoted at 95% confidence level. Zircon U–Pb age data are listed in Supplementary Table 1.

Hf isotopic analyses were carried on the same zircon grains that were previously analyzed for U–Pb ages, using a Neptune MC-ICP-MS, equipped with a 193 nm laser, at Tianjin Institute of Geology and Mineral Resources. Most analyses are carried out with a beam diameter of 50 μm, a 10 Hz repetition rate, and energies of 100 mJ per pulse. The detailed analytical techniques were similar to those described in detail by Wu et al. (2006). Zircon Hf isotope data are presented in Supplementary Table 2.

Zircon oxygen isotopes were measured using the Cameca IMS 1280 SIMS at the Institute of Geology and Geophysics, Chinese Academy of Sciences in Beijing. The detailed analytical procedures are the same as those described by Li et al. (2010a). The Cs^+ primary ion beam was accelerated at 10 KV, with an intensity of ca. 2 nA and rastered over a 10 μm area. The spot is about 20 μm in diameter. The instrumental mass fractionation factor (IMF) is corrected using Penglai zircon standard with $(\delta^{18}O)_{VSMOW} = 5.31‰$ (Li et al., 2010b). Measured $^{18}O/^{16}O$ is normalized by using Vienna Standard Mean Ocean Water compositions (VSMOW). Ten measurements of the Qinghu zircon standard during the course yield a weighted mean of $\delta^{18}O = 5.44 \pm 0.21‰$ (2SD), which is consistent

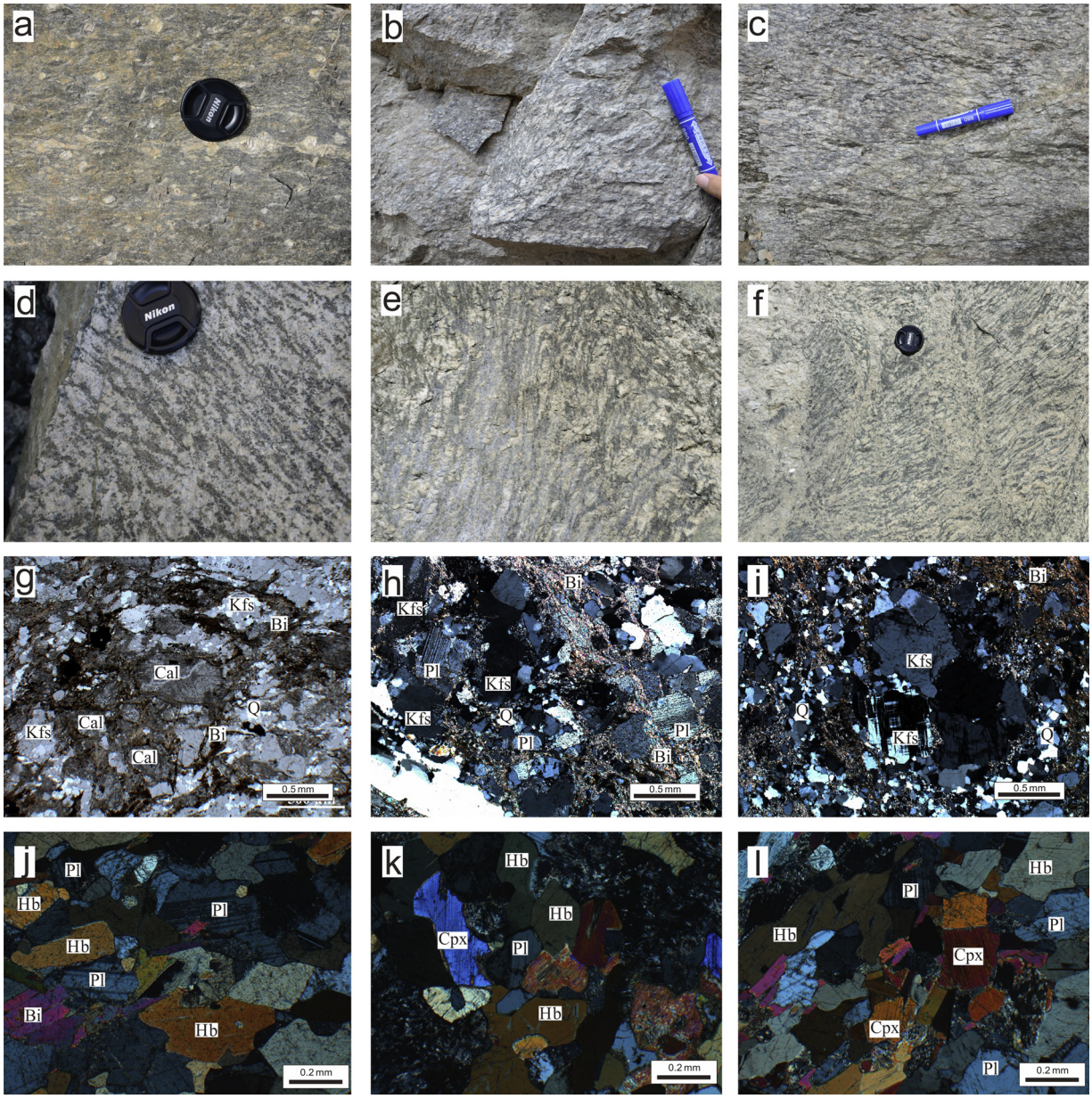

Fig. 3. Representative field photographs and photomicrographs of migmatite and granites from the Azibailedi pluton. (a) The banded migmatite is composed of quartz and feldspar phenocrysts. (b, c) The biotite monzogranites show gneissic textures. (d–f) The granites show medium to coarse granitic and strong gneissic structures. (g) The mineral assemblage of the migmatite (parallel nicols). (h–i) The recrystallization of quartz and biotite possibly represent metamorphic effect (crossed nicols). (j) The mineral assemblage of the amphibolites from the Heluositan Complex (crossed nicols). (k, l) Relict clinopyroxene in amphibolites (crossed nicols). *Abbreviations*: Cal, carbonate; Kfs, K-feldspar; Pl, plagioclase; Bi, biotite; Q, quartz; Hb, hornblende; Cpx, clinopyroxene.

within errors with the reported value of 5.4 ± 0.2‰ (Li et al., 2013). Zircon oxygen isotopic data are listed in Supplementary Table 3.

Major elements were measured by Rigaku ZSX100e X-ray fluorescence spectrometer (XRF) at the State Key Laboratory of Isotope Geochemistry, Guangzhou Institute of Geochemistry, Chinese Academy of Sciences (CAS). Whole rock samples were crushed and powdered to less than 200 mesh in an agate mill, and then fused lithium-tetraborate glass pellets. Analytical precision as determined on the Chinese National standard GSR-1 and GSR-3 were generally around 1–5%. Trace elements were analyzed using a Perkin-Elmer ELAN-DRC-e inductively-coupled plasma mass spectrometry (ICP-MS) at the State Key Laboratory of Ore Deposit Geochemistry, Institute of Geochemistry, CAS. The powdered samples (50 mg) were digested in high-pressure Teflon bombs using $HF + HNO_3$ mixture for 48 hours at about 195 °C (Qi et al., 2000). The analytical precision for most elements was better than 3–5%. The analytical results are presented in Table 1.

Samples for Nd–Sr isotopic measurements were spiked and dissolved in Teflon bombs with $HF + HNO_3$ acid, and then separated by conventional cation-exchange techniques. The isotopic measurements were performed on a Thermo Fisher Triton TI mass spectrometer (TIMS) at the State Key Laboratory of Ore Deposit Geochemistry, Institute of Geochemistry, CAS. The detail procedure is as described by Li et al. (2004). The measured $^{87}Sr/^{86}Sr$ and $^{143}Nd/^{144}Nd$ ratios are corrected to $^{86}Sr/^{88}Sr = 0.1194$ and $^{146}Nd/^{144}Nd = 0.7219$, respectively. The report $^{87}Sr/^{86}Sr$ average ratios for NBS987 standard and BCR-2 were $^{87}Sr/^{86}Sr = 0.710219 \pm 5$ (2σ) and 0.704966 ± 3 (2σ), respectively, and $^{143}Nd/^{144}Nd$ average

Table 1
Geochemical compositions of the Azibailedi granite pluton.

Sample	13TR02H1	13TR02H2	13TR02H3	13TR02H4	13TR02H5	13TR02H6	13TR02H7	13TR03H1	13TR03H2	13TR03H3	13TR03H5	13TR03H6
Major elements (%)												
SiO_2	74.0	75.1	72.8	73.2	73.3	73.6	74.4	73.1	73.7	75.1	73.5	74.2
TiO_2	0.34	0.27	0.35	0.30	0.39	0.27	0.32	0.31	0.32	0.30	0.27	0.31
Al_2O_3	15.9	12.0	12.4	12.0	12.4	11.1	12.3	12.0	12.4	12.2	12.3	11.8
$Fe_2O_3^T$	2.41	2.42	2.97	2.32	2.89	2.90	2.78	2.46	2.67	2.09	2.31	2.73
MnO	0.04	0.04	0.04	0.03	0.03	0.04	0.03	0.04	0.05	0.03	0.04	0.04
MgO	0.39	0.45	0.44	0.68	0.87	0.76	0.55	0.42	0.30	0.52	0.29	0.40
CaO	1.55	0.50	0.82	0.43	0.20	0.53	0.31	0.60	0.87	0.42	0.91	0.82
Na_2O	2.11	2.47	2.00	3.74	2.67	2.44	2.17	4.08	2.72	2.82	3.01	2.14
K_2O	5.65	5.45	6.22	5.92	5.92	6.56	6.02	5.68	5.52	5.40	5.67	5.98
P_2O_5	0.05	0.04	0.05	0.05	0.07	0.04	0.04	0.04	0.04	0.04	0.04	0.04
LOI	1.00	0.96	1.51	1.04	0.80	1.41	0.79	0.97	1.07	0.68	1.25	1.22
Total	103.4	99.7	99.7	99.7	99.6	99.7	99.7	99.7	99.7	99.7	99.7	99.7
A/CNK	1.28	1.10	1.08	0.90	1.11	0.92	1.15	0.86	1.03	1.09	0.97	1.03
Trace elements (ppm)												
Sc	11.8	10.8	13.2	9.81	11.3	10.4	12.5	12.7	12.1	11.7	10.7	11.8
V	11.3	8.48	10.1	10.5	12.6	9.37	9.05	9.43	9.07	7.26	8.37	8.75
Cr	4.91	4.24	4.45	3.88	5.59	3.95	4.98	3.57	4.13	3.43	3.60	5.46
Co	1.94	1.57	1.68	1.66	1.75	1.34	1.52	1.63	1.64	0.988	1.55	1.34
Ni	3.99	3.17	1.72	1.28	2.37	1.20	1.64	1.38	1.41	1.42	1.31	1.62
Cu	3.20	3.95	10.27	3.99	3.58	2.74	4.89	12.66	6.55	3.53	8.14	3.05
Zn	50.1	52	83.4	40.7	60.1	77.2	70.2	58.6	64.2	63.5	59.5	57.8
Ga	17.4	18.3	19.5	18.0	18.8	19.8	19.5	18.0	19.6	18.0	19.2	16.7
Rb	210	207	240	219	282	316	288	248	226	228	209	257
Sr	53.1	42.4	46.1	40.8	31.4	23	35.7	43.9	60.3	32.9	53.6	35.4
Y	46.4	49.1	54.1	53.1	58.7	57.4	61.5	50.8	56.9	57.8	49.1	68.4
Zr	264	258	301	253	287	225	278	311	265	272	230	292
Nb	23.9	22.7	27.9	20.6	25.6	21.5	29.0	25.1	27.2	26.8	21.1	26.1
Cs	6.25	2.22	4.48	3.01	8.11	6.24	6.65	8.60	7.36	4.64	2.81	4.26
Ba	836	716	887	697	784	866	743	697	799	743	858	907
La	59.3	66.4	64.4	76.0	77.0	92.0	90.3	57.1	68.4	79.6	78.1	106
Ce	120	133	129	156	154	184	182	115	137	162	160	218
Pr	13.2	14.4	14.3	16.7	16.7	19.5	19.5	12.8	14.9	17.2	17.3	22.8
Nd	49.1	52.3	53.1	60.2	60.4	69.1	69.7	48.0	54.8	62.4	62.6	83.6
Sm	8.82	9.40	9.77	11.3	10.9	11.9	12.5	9.15	9.90	11.2	11.1	14.9
Eu	0.812	0.645	0.991	0.722	0.741	1.02	0.997	0.845	0.949	0.887	0.846	1.38
Gd	8.45	8.85	9.40	10.2	10.4	10.7	10.9	8.99	9.65	10.4	9.53	13.3
Tb	1.37	1.45	1.54	1.72	1.74	1.72	1.84	1.43	1.62	1.76	1.64	2.18
Dy	7.93	8.19	8.91	9.76	10.00	9.63	10.40	8.51	9.58	10.20	9.25	12.7
Ho	1.64	1.68	1.91	1.96	2.02	1.92	2.10	1.75	2.00	2.09	1.87	2.59
Er	4.80	4.97	5.61	5.54	5.85	5.78	6.23	5.20	6.02	6.23	5.67	7.71
Tm	0.702	0.712	0.797	0.743	0.808	0.844	0.894	0.762	0.871	0.893	0.800	1.10
Yb	4.33	4.62	5.42	4.48	5.09	5.29	5.67	4.72	5.70	5.72	5.08	7.06
Lu	0.639	0.670	0.780	0.627	0.711	0.755	0.840	0.696	0.838	0.826	0.733	1.02
Hf	7.38	7.23	8.25	6.71	7.51	6.28	7.55	8.29	7.17	7.82	7.18	8.88
Ta	1.58	2.01	1.84	1.08	2.01	1.52	1.88	1.74	1.89	1.86	1.57	1.91
Pb	21.7	31.5	34.9	22.9	13.8	17.0	22.4	25.5	27.9	23.1	29.5	26.3
Th	22.8	26.0	21.6	28.4	27.3	26.0	29.1	20.4	27.3	26.6	25.7	30.7
U	3.60	3.53	3.80	3.13	3.22	3.53	3.73	4.38	4.09	5.27	6.54	3.48
T_{Zr} (°C)	853	837	847	809	846	802	848	822	830	841	810	840

ratios for LRIG and BCR-2 were $^{143}Nd/^{144}Nd = 0.512196 \pm 3$ (2σ) and 0.512634 ± 4 (2σ), respectively. The analytical results and calculated parameters are listed in Table 2.

5. Results

5.1. U–Pb zircon geochronology

5.1.1. The Azibailedi pluton (migmatite sample 13TR01: N 37°54.70′, E 76°16.78′; gneissic granite samples 13TR02: N 37°55.31′, E 76°16.15′ and 13TR03: N 37°55.64′, E 76°16.17′)

Zircons from the three samples are prismatic and colorless, with lengths of 100–150 μm and length to width ratios between 1 and 2. In CL images, internal growth zoning is clear in most zircon crystals and no core-rim structure has been observed (Fig. 4). Total 30 analyses from 13TR01 show large range of U and Th concentrations (U = 135–1095 ppm, Th = 57–361 ppm) with Th/U ratios ranging from 0.23 to 0.62 (Supplementary Table 1). The measured $^{206}Pb/^{238}U$ ages are in good agreement within analytical errors, and yield a weighted mean age of 1414 ± 3 Ma (MSWD = 1.7; Fig. 5a). The data from sample 13TR02 yield variable concentrations of U (189–3629 ppm) and Th (86–1923 ppm), with Th/U ratios of 0.26–0.83 (Supplementary Table 1). The data yield a well-defined discordia with upper intercept age of 1405 ± 9 Ma, which is consistent with the weighted mean $^{207}Pb/^{206}Pb$ age of 1405 ± 6 Ma (MSWD = 0.76; Fig. 5b). The features and U, Th contents of sample 13TR03 are similar to those of the sample 13TR02. Due to variable radiogenic Pb loss, most analyses yield discordant $^{206}Pb/^{238}U$ and $^{207}Pb/^{235}U$ ages. However, all the analyses define a discordia with an upper intercept age of 1412 ± 12 Ma (MSWD = 3.5; Fig. 5c). Their consistent $^{207}Pb/^{206}Pb$ ages yield a weight mean age of 1401 ± 5 Ma (MSWD = 0.77; Fig. 5c). The ca. 1.4 Ga age obtained from these samples is regarded as the best estimate of the crystallization age of the Azibailedi pluton.

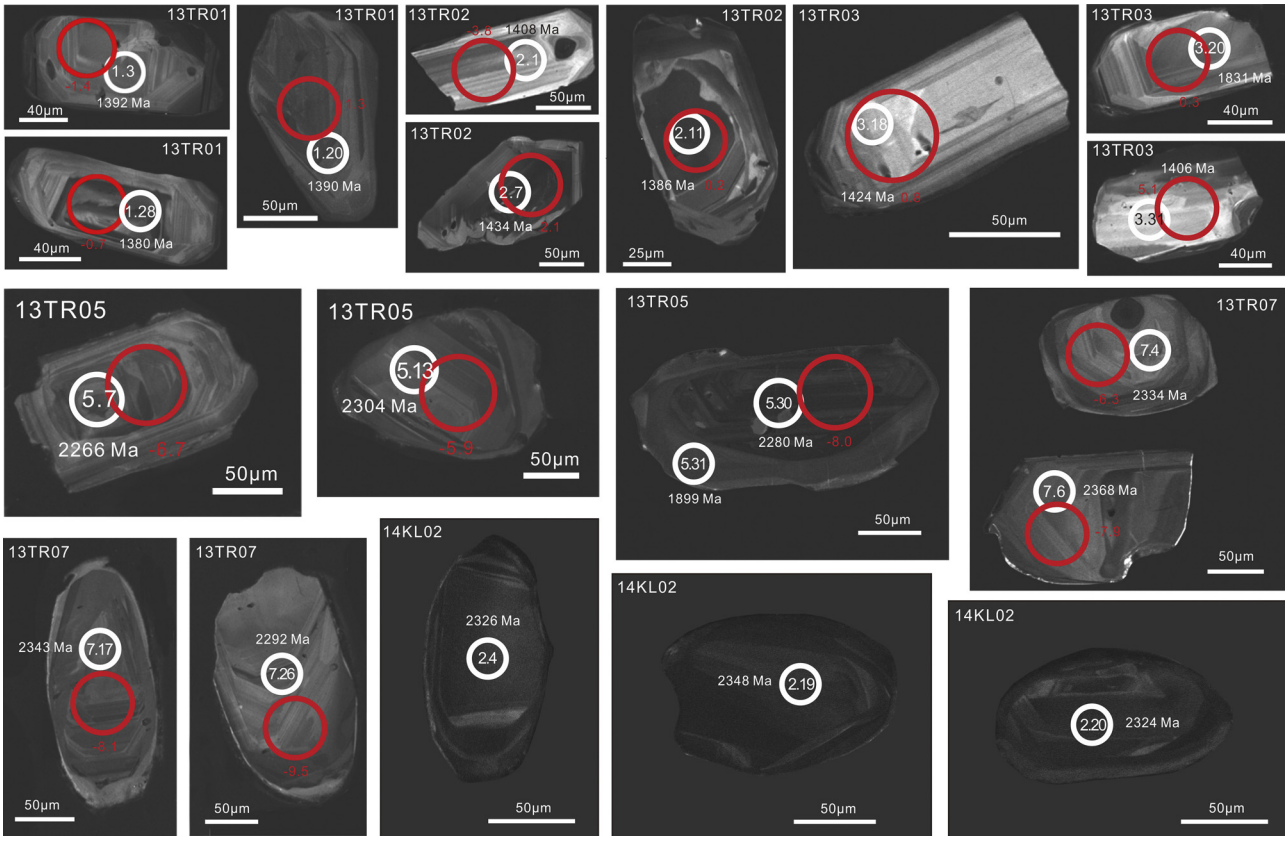

Fig. 4. Representative CL images of zircons from the Azibailedi pluton, Akazi pluton and amphibolites, Analytical spots, ages and $\varepsilon_{Hf}(t)$ values are shown.

5.1.2. The Heluositan complex (granitic gneiss sample 13TR05: N 37°05.19′, E 76°53.37′; gneissic granite sample 13TR07: N 37°05.45′, E 76°56.15′; and amphibolite: 14KL02: N 37°07.52′, E 76°52.31′)

Zircons from the sample 13TR05 are largely euhedral and light pink-colored, with the length ranging from 100 μm to 200 μm and length to width ratio of 2–3. Euhedral concentric zoning is common in most crystals and a few crystals display core-rim structures. The rims are more luminescent than the cores (Fig. 4). Among the 25 analyses, 21 were carried out on the cores and the results show variable U and Th contents (U = 273–929 ppm, Th = 158–660 ppm, Th/U = 0.48–0.75, Supplementary Table 1). Due to variable radiogenic Pb loss, most analyses yield discordant $^{206}Pb/^{238}U$ and $^{207}Pb/^{235}U$ ages and fall along a discordia with upper intercept age of 2386 ± 56 Ma (Fig. 5d). The other 4 analyses on the rims have large range of U and Th contents and Th/U ratios (U = 193–864 ppm, Th = 54–1115 ppm, Th/U = 0.28–1.29, see Supplementary Table 1). These four analyses are close to the concordia and yield a weight mean $^{207}Pb/^{206}Pb$ age of 1896 ± 66 Ma (MSWD = 11.4). Although this age shows large error and MSWD, it is consistent with the previously reported more precise metamorphic age of 1917 ± 7 Ma (MSWD = 1.2, n = 8) obtained by SHRIMP method (Zhang et al., 2007a).

Zircons from sample 13TR07 share most features similar to those in sample 13TR05 except for the thinner rims. They are transparent and pinkish in color, euhedral prismatic with concentric zonings in CL images. The grains show length varying from 150 to 200 μm and length to width ratio of 2–3 (Fig. 4). Twenty-five analyses were performed on 30 zircon grains. The data show variable abundance of U (47–559 ppm) and Th (36–307 ppm) and Th/U ratios of 0.22–0.76 (Supplementary Table 1). All analyses yield discordant $^{206}Pb/^{238}U$ and $^{207}Pb/^{235}U$ ages due to variable radiogenic Pb loss. Thus, we regard the upper intercept age of 2365 ± 32 Ma (MSWD = 3.4) as the best estimation of the crystallization age of this sample (Fig. 5e).

Zircons in sample 14KL02 are euhedral and colorless, up to 50–100 μm long and have length/width ratios of 1–2. All the zircon grains are transparent and pinkish in color, euhedral prismatic without obvious zoning and show dark color under CL (Fig. 4). The analytical results listed in Supplementary Table 1 show variable U (188–1406 ppm) and Th (73–1223 ppm) contents with Th/U ratios between 0.39 and 0.87. Similar with the scenario of zircons in the samples 13TR05 and 13TR07, all the analyses show variable radiogenic Pb loss but fall along a well-defined discordia with an upper intercept age of 2339 ± 13 Ma (MSWD = 1.1) (Fig. 5f). The $^{207}Pb/^{206}Pb$ ages are consistent within error and yield a weight mean age of 2346 ± 12 Ma (MSWD = 1.9) (Fig. 5f), comparable with the upper intercept age.

In summary, the zircon U–Pb ages for the gneissic granites and amphibolite suggest that the Heluositan complex crystallized at 2.3–2.4 Ga and underwent metamorphism at ca. 1.9 Ga, which is consistent with previous geochronological data from the Heluositan complex, within analytical errors (Wang et al., 2014; Zhang et al., 2007a).

5.2. Whole-rock geochemistry

The granites from the Azibailedi pluton are siliceous with a restricted range in SiO_2 content from 72.8% to 75.1% (Table 1). The rocks have high total alkalis with $Na_2O + K_2O$ between 7.40% and 10.63% and K_2O (5.40–6.56%) is higher than Na_2O (2.00–4.08%). Based on Streickeisen classification, the rocks correspond to monzogranite (Fig. 6a), which is also consistent with petrographic observations. They show peralkaline through metaluminous to weakly peraluminous nature with A/CNK values from 0.86 to 1.15 and display a positive correlation between

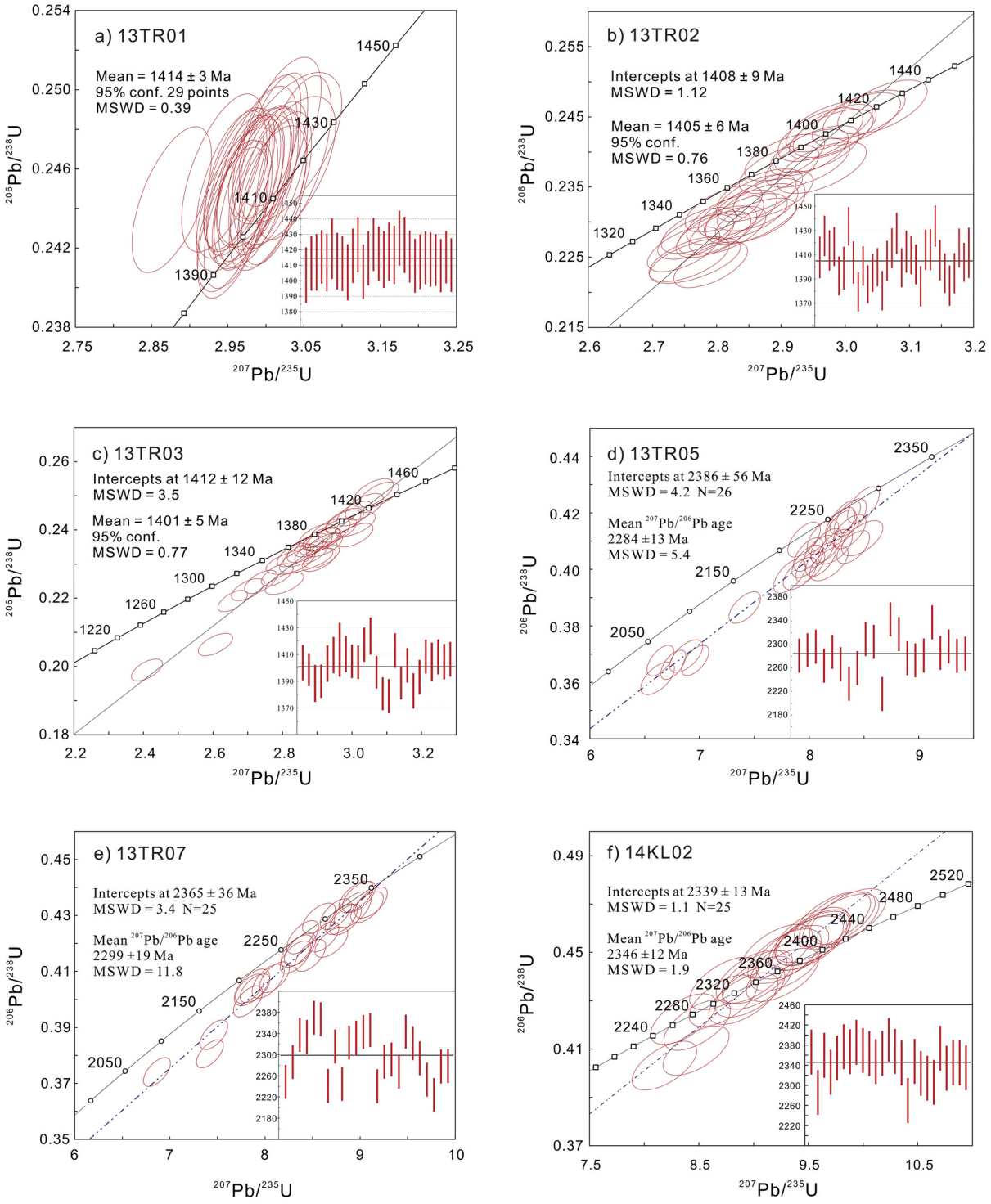

Fig. 5. Concordia plots of U–Pb zircon data for zircons from the Azibailedi granites and Heluositan Complex.

A/NK and A/CNK values suggesting fractionation of plagioclase (Fig. 6b; Maniar and Piccoli, 1989). Most of the samples are alkali-calcic and ferroan on the MALI vs. SiO_2 and Fe* vs. SiO_2 diagrams, respectively (Fig. 6c, d; Frost et al., 2001; Frost and Frost, 2008).

The Azibailedi granites have high total REE contents ranging from 275 ppm to 494 ppm (Table 1). On the chondrite-normalized patterns (chondrite values are from Boynton (1984)), they show markedly LREE-enriched patterns with $(La/Yb)_N$ ranging from 8.5 to 12.2, significant negative Eu anomalies ($\delta Eu = 0.21–0.32$), and relatively flat HREE patterns ($(Gd/Yb)_N = 1.4–1.9$) (Fig. 7a). Normalized to primitive mantle (primitive mantle values are from Sun and McDonough (1989)), all the granitic rocks show prominent negative Nb, Ta, Sr, P, and Ti anomalies (Fig. 7b).

5.3. Whole-rock Sr–Nd isotopic compositions

Strontium and neodymium isotopic compositions of the representative granite samples are listed in Table 2. The samples from the Azibailedi pluton show constant values of $^{147}Sm/^{144}Nd$

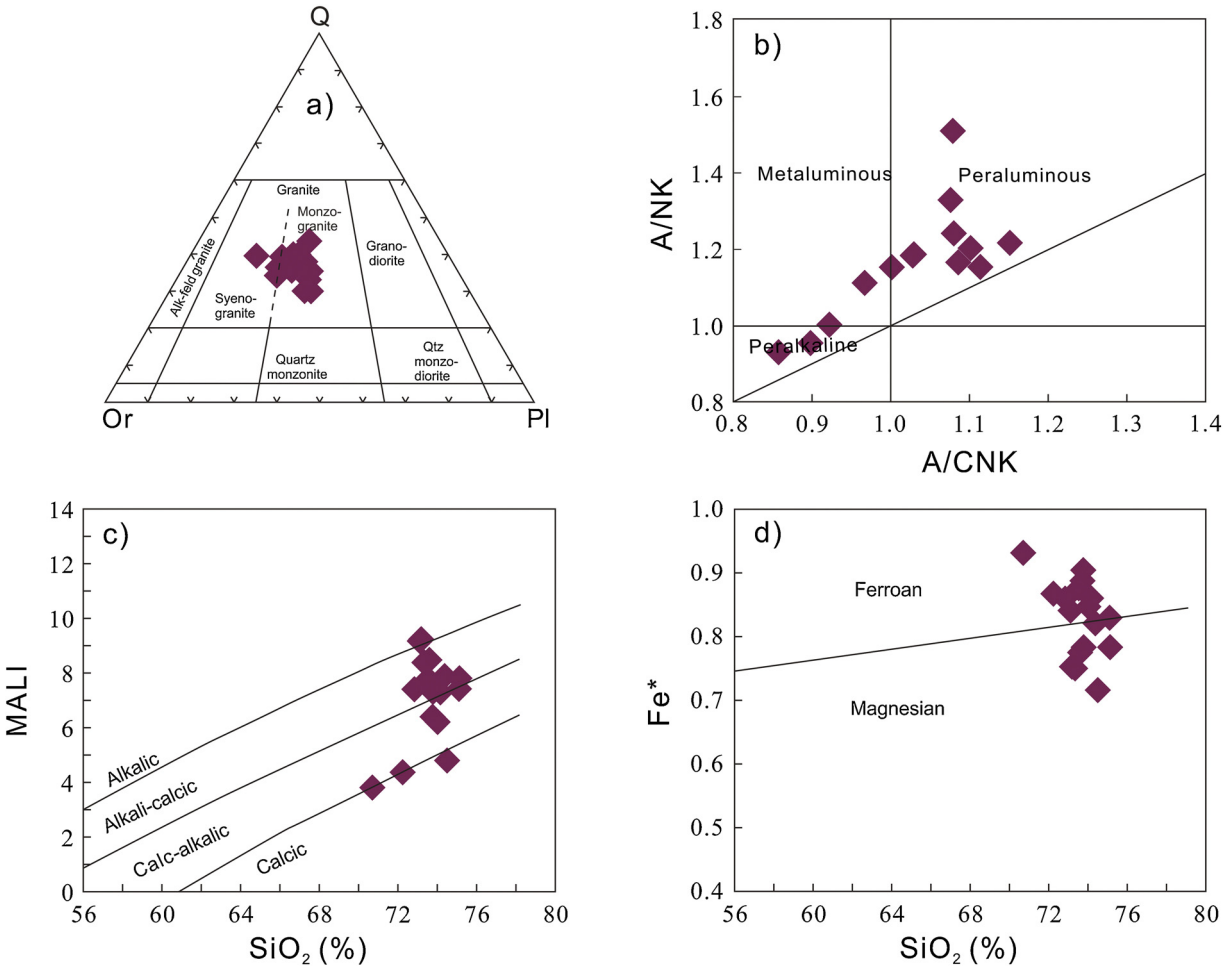

Fig. 6. (a) Normalized Q-A-P classification diagram showing the granites from the Azibaledier pluton is monzogranite. (b) A/NK vs. A/CNK plot (Maniar and Piccoli, 1989). (c) MALI vs. SiO_2 (%) and (d) Fe* vs. SiO_2 (%) plot (Frost et al., 2001; Frost and Frost, 2008). A = Al_2O_3, N = Na_2O, K = K_2O, C = CaO (all in molar proportion); MALI = $Na_2O + K_2O - CaO$ (%); Fe* = $FeO^t/(MgO + FeO^t)$ (%).

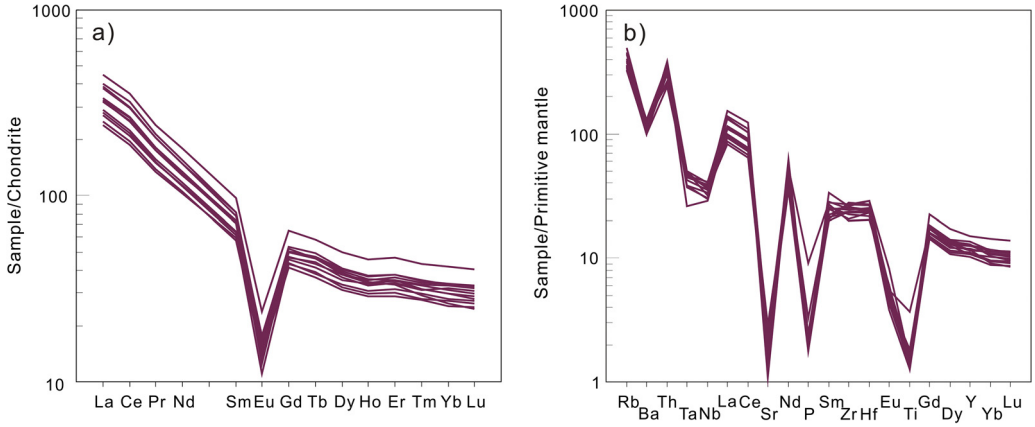

Fig. 7. (a) Chondrite-normalized rare earth element (REE) patterns and (b) primitive mantle-normalized trace element spider diagram for Azibailedi A-type granites.

(0.1072–0.1112) and $^{143}Nd/^{144}Nd$ (0.511640–0.511717), corresponding to relatively homogeneous initial $^{143}Nd/^{144}Nd$ ratios (0.510663–0.510719) and $\varepsilon_{Nd}(t)$ values (−3.5 to −2.2) (Fig. 8) and with a restricted range of $T_{DM}{}^{C}$ from 2.26 Ga to 2.38 Ga. Their Rb–Sr isotopic compositions are quite variable with initial $^{87}Sr/^{86}Sr$ ratios ranging from 0.54422 to 0.70303. They show abnormally low $(^{87}Sr/^{86}Sr)_i$ ratios due to their high $^{87}Sr/^{86}Sr$ ratios (up to 11). Thus, the ratios cannot be considered as true initial Sr isotopic compositions (Jahn, 2004; Wu et al., 2002).

5.4. Zircon Hf–O isotopes

Almost all the dated zircon grains were also measured for their Lu–Hf isotope compositions and the results are listed in Supplementary Table 2 (the calculation formula and the relevant constant used in calculations are presented in the footnote of this table).

Zircons from the Azibailedi granites have a range of initial $^{176}Hf/^{177}Hf$ ratios (0.281782–0.282187) (Fig. 9a), yielding a large range of $\varepsilon_{Hf}(t)$ values from −4.1 to +6.1 (Fig. 9b) with weight mean

Table 2
Sr–Nd isotopic compositions of the granites.

Sample	Rock type	Rb (ppm)	Sr (ppm)	$^{87}Rb/^{86}Sr$	$^{87}Sr/^{86}Sr$ (2σ)	$(^{87}Sr/^{86}Sr)_i$	Sm (ppm)	Nd (ppm)	$^{147}Sm/^{144}Nd$	$^{143}Nd/^{144}Nd$ (2σ)	$(^{143}Nd/^{144}Nd)_i$	$\varepsilon_{Nd}(t)$	T_{2DM} (Ga)
13TR02H1	Granite	210	53.1	11.69	0.926771 (8)	0.69209	8.82	49.1	0.1086	0.511717 (8)	0.510719	−2.2	2.26
13TR02H3	Granite	240	46.1	15.40	0.936298 (12)	0.62708	9.77	53.1	0.1112	0.511714 (6)	0.510691	−2.7	2.27
13TR02H5	Granite	282	31.4	26.72	0.997400 (14)	0.46086	10.9	60.4	0.1091	0.511666 (4)	0.510663	−3.3	2.34
13TR02H7	Granite	288	35.7	24.10	1.039874 (12)	0.55598	12.5	69.7	0.1084	0.511660 (8)	0.510663	−3.2	2.35
13TR03H5	Granite	209	53.6	11.53	0.934587 (18)	0.70303	11.1	62.6	0.1072	0.511652 (4)	0.510666	−3.2	2.36
13TR03H6	Granite	257	35.4	21.56	0.977102 (12)	0.54422	14.9	83.6	0.1077	0.511640 (10)	0.510649	−3.5	2.38
BCR-2 (n = 2)					0.704966 (6)					0.512634 (8)			
LRIG (n = 2)										0.512196 (6)			
NBS987 (n = 3)					0.710219 (10)								

Chondrite uniform reservoir (CHUR) values ($^{87}Rb/^{86}Sr$ = 0.0847, $^{87}Sr/^{86}Sr$ = 0.7045; $^{147}Sm/^{144}Nd$ = 0.1967, $^{143}Nd/^{144}Nd$ = 0.512638) are used for the calculation. λ_{Sm} = 6.54 × 10^{-12} $year^{-1}$ (Lugmair and Harti, 1978). The $(^{87}Sr/^{86}Sr)_i$, $(^{143}Nd/^{144}Nd)_i$, $\varepsilon_{Nd}(t)$ of the Azibailedi granites were calculated using age of 1400 Ma. The two-stage model age (T_{2DM}) calculations are given by Jahn et al. (1999).

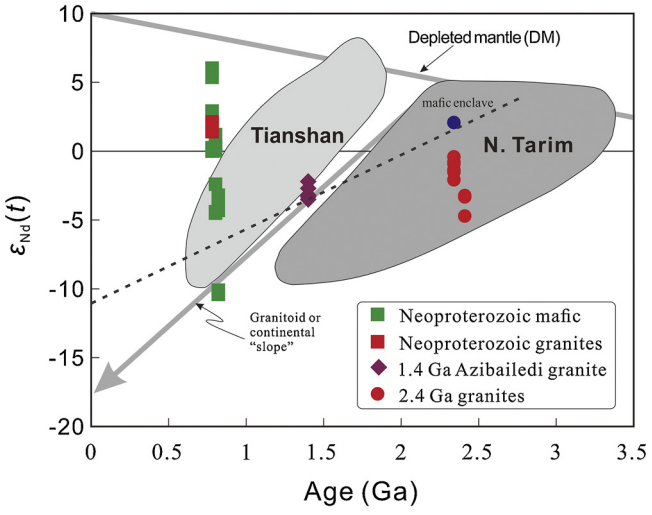

Fig. 8. Whole rock $\varepsilon_{Nd}(t)$ vs. crystallization age of the igneous rocks from the southwestern margin of the Tarim Craton.
Data are from Hu et al. (2000), Zhang et al. (2003, 2004, 2006a,b, 2007a,b, 2010).

$\varepsilon_{Hf}(t)$ of 1.26 (Fig. 10a). The two-stage Hf model ages (T_{DM}^{C}) range from 1.93 Ga to 2.82 Ga (mostly 2.16 Ga to 2.66 Ga) with weighted mean value of 2.37 Ga (Fig. 10b) which is identical with two-stage Nd model ages.

The measured $^{176}Hf/^{177}Hf$ ratios of granite samples from the Heluositan complex range from 0.281016 to 0.281302, corresponding to initial $^{176}Hf/^{177}Hf$ ratios of 0.280987 to 0.281273 (Fig. 9a) and $\varepsilon_{Hf}(t)$ values of −11.0 to −3.1 (Fig. 9b). The weighted mean $\varepsilon_{Hf}(t)$ value is −7.8 and two-stage Hf model ages (T_{DM}^{C}) range from 3.29 Ga to 3.98 Ga (Fig. 10c, d).

The O isotope values of the fifty-one zircons of the Azibailedi granites are fairly homogeneous. The measured zircon $\delta^{18}O$ values range from 7.1‰ to 8.7‰ (with the exception of one analysis which is up to 10.1‰ due to unknown reason). The data define a Gaussian distribution (Fig. 11a) with a peak at 7.9 ± 0.1‰ (2SD) (Fig. 11a), which is higher than the normal mantle zircon values of 5.3 ± 0.6‰ (2SD) (Valley et al., 1998, 2005) (Fig. 11b).

6. Discussion

6.1. Classification of the Azibailedi pluton

Granitoids are generally divided into I-, S-, A- and M-types according to the nature of protolith and pressure-temperature conditions of melting (Bonin, 2007). Several attempts have been made to distinguish A-type granites from other types (Eby, 1990; Loiselle and Wones, 1979; Whalen et al., 1987). Among these, the characteristics of high $Na_2O + K_2O$, Fe/Mg (in molar) and Ga/Al ratios, low CaO content, enrichment in HFSEs and depletion in Sr, Eu have been considered a significant role to discriminate A-type granites (Bonin, 2007; Collins et al., 1982; King et al., 1997; Loiselle and Wones, 1979; Whalen et al., 1987). In the Zr vs. 10,000 × Ga/Al diagram (after Whalen et al., 1987), the rocks from the Azibailedi pluton fall in the A-type field (Fig. 12a). On the other hand, the FeO*/MgO vs. (Zr + Nb + Ce + Y) relation has been used to discriminate A-type granites and highly differentiated granites (e.g. Zhao et al., 2008). All the samples from the pluton plot in the A-type field (Fig. 12b). The above mentioned features reveal the typical A-type signature of the Azibailedi granites, and further classify as A_2-type according to the scheme of Eby (1992) (Fig. 12c, d).

The negative correlation between Zr and SiO_2 (figure not shown) indicates that the magma was saturated in Zr, consistent with zircon separation from the residual magma during crystallization.

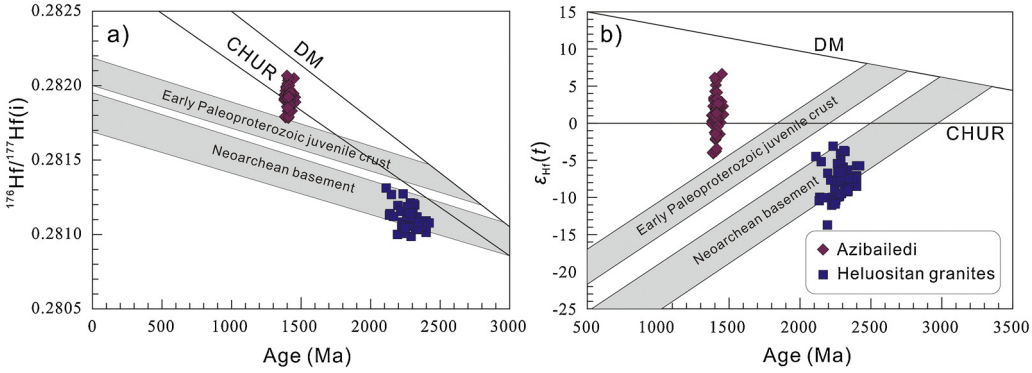

Fig. 9. (a) Zircon initial $^{176}Hf/^{177}Hf(i)$ and (b) $\varepsilon_{Hf}(t)$ vs. crystallization age of the Azibailedi and Akazi pluton.

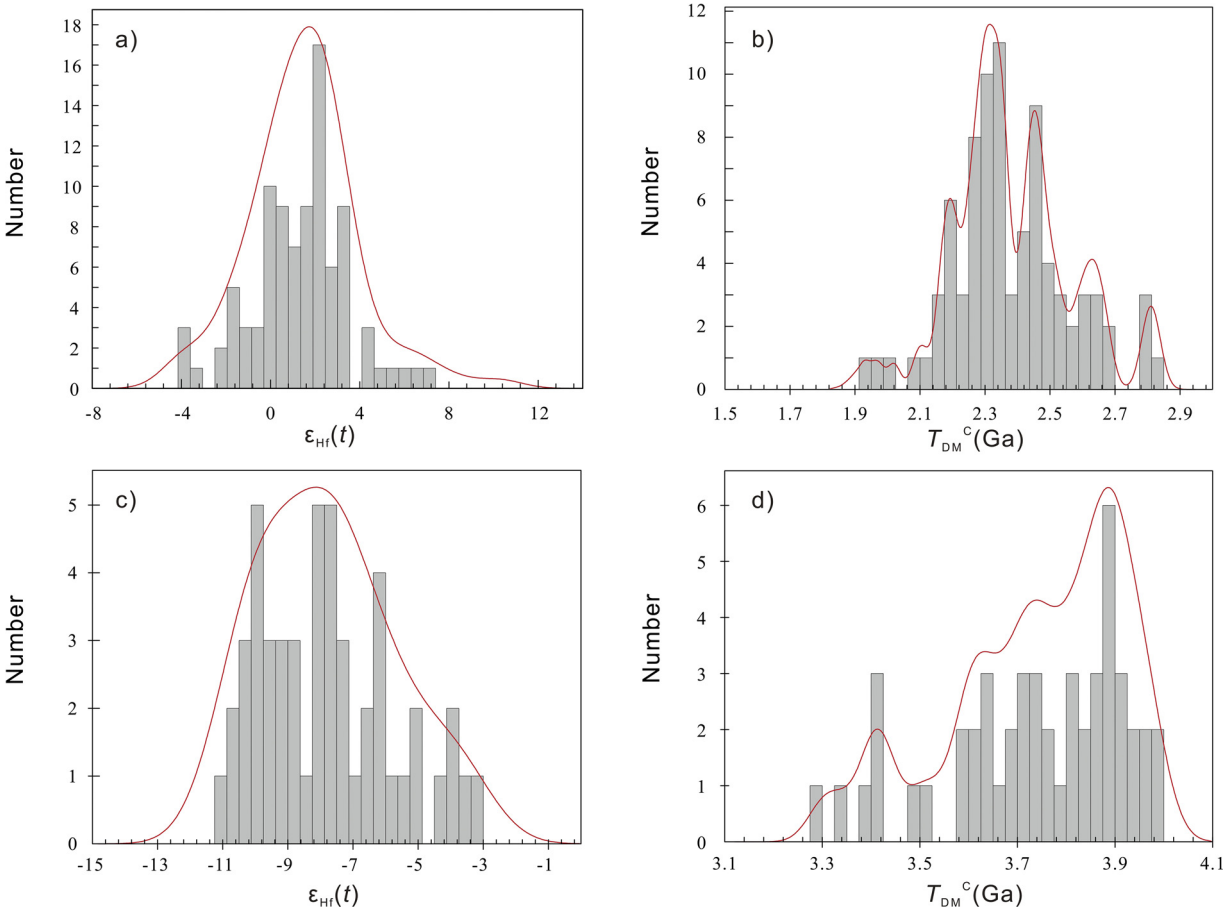

Fig. 10. Histograms of zircon $\varepsilon_{Hf}(t)$ and T_{DM}^{C} for the rocks of the Azibailedi pluton and granitic gneisses from Heluositan Complex.

Zircon saturation thermometry provides a minimum estimation of magma temperature (Jung et al., 2000; Miller et al., 2003; Watson and Harrison, 1983). The calculated zircon saturation temperatures (T_{Zr}) of the Azibailedi granites range from 802 °C to 853 °C (Table 1) with a weighted average of 832 °C. Thus, the relatively high temperature further supports the A-type signature of the Azibailedi granites (Bonin, 2007; Zhu et al., 2010).

6.2. Petrogenesis of the Azibailedi pluton

A number of magmatic processes have been proposed to interpret the formation of A-type granites since the term was introduced by Loiselle and Wones (1979), including extensive fractional crystallization of a mantle-derived mafic magma with or without crustal contamination (Anderson et al., 2003; Eby, 1990; Han et al., 1997; Zhang and Zou, 2013; Zhong et al., 2007), magma mixing between basaltic and crustal melts (Dall'Agnol and de Oliveira, 2007; Heilimo et al., 2014; Yang et al., 2006; Zhu et al., 2010) and partial melting of the crust (Huang et al., 2008; Jung et al., 1998, 2000).

Closed system fractionation crystallization of a mantle-derived mafic magma is excluded because of the following features: (1) the absence of either contemporary (1.4 Ga) mafic or intermediate magmatic rocks in the area, (2) fairly broad range in $\varepsilon_{Hf}(t)$ values (−4.1 to +6.1) of the Azibailedi granite samples, (3) high zircon $\delta^{18}O$ values (7.1–8.7‰), obviously higher than that of the mantle values (Fig. 11b) and (4) absence of a continuous compositional trend from mafic through intermediate to felsic rocks, which

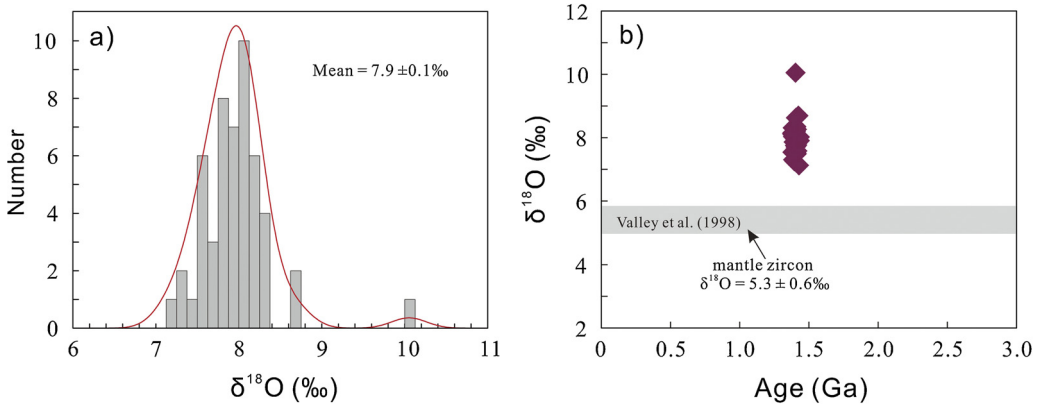

Fig. 11. (a) Histogram of single zircon $\delta^{18}O$ values for the Azibailedi granites. (b) single zircon $\delta^{18}O$ data vs. $^{207}Pb/^{206}Pb$ ages for the Azibailedi granites. Field of mantle zircon is from Valley et al. (1998).

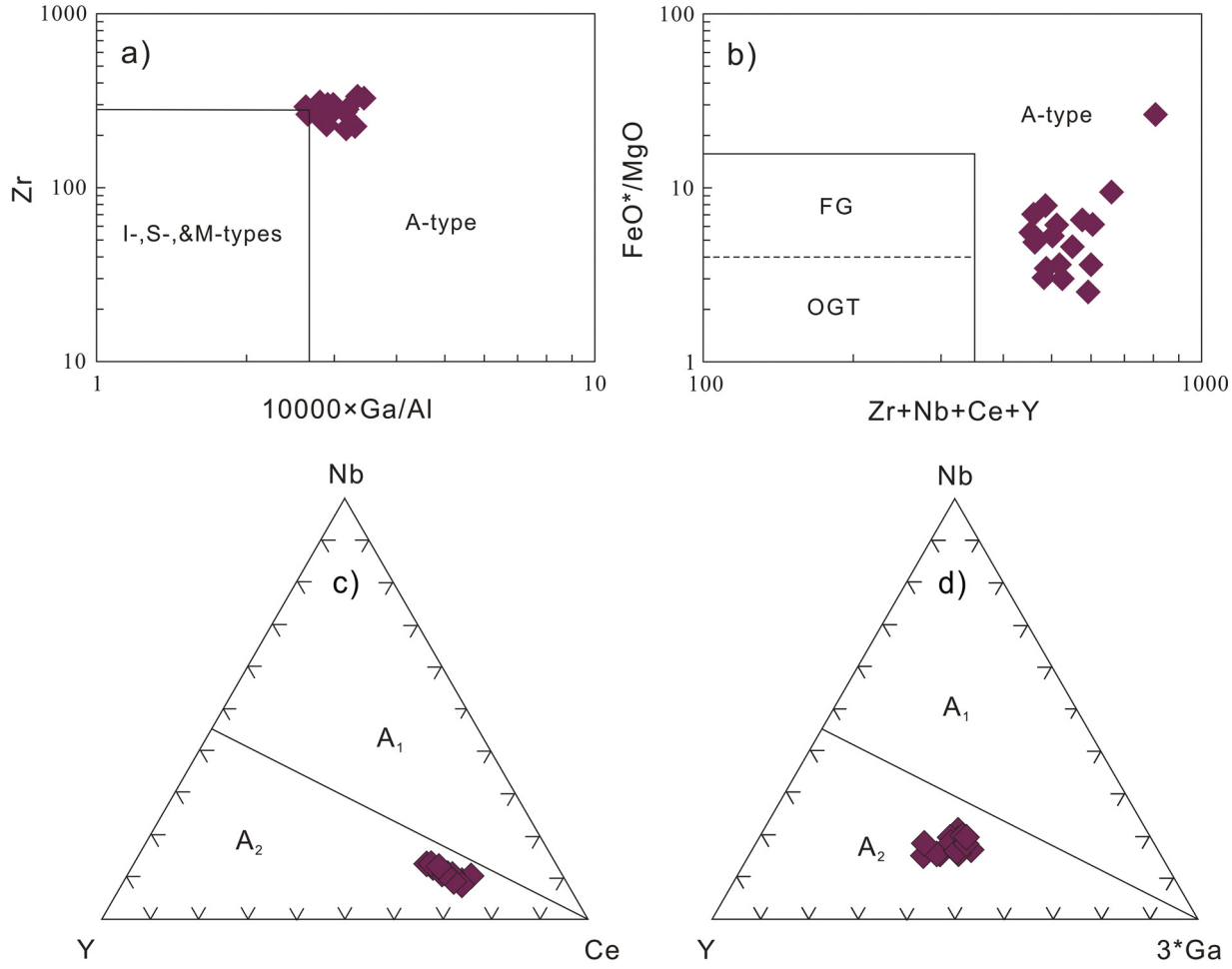

Fig. 12. (a) Zr vs. 10,000 × Ga/Al and (b) FeO*/MgO vs. (Zr + Nb + Ce + Y) discrimination diagrams of Whalen et al. (1987), indicative of the Azibailedi pluton is an A-type granite. Plots of (c) Y–Nb–Ce and (d) Y–Nb–3 × Ga show Azibailedi granites are A_2-type granites (Eby, 1992). FG, fractionated felsic granites; OGT, unfractionated; A1, anorogenic A-type granites; A2, post-collisional A-type granites.

is a general feature of A-type magmatic suites derived from fractional crystallization (Wang et al., 2010; Zhang and Zou, 2013). Although the A-type granites have broad range in $\varepsilon_{Hf}(t)$ values, the constant $\delta^{18}O$ ratios and $\varepsilon_{Nd}(t)$ values suggest that magma mixing is also unlikely to explain the petrogenesis of the Azibailedi granites. Furthermore, the absence of any mafic microgranular enclaves (MMEs) in the Azibailedi pluton also rules out the mixing model (Rudnick and Gao, 2003; Renjith et al., 2014; He et al., 2015a,b).

Consequently, partial melting of mafic crustal rocks at shallow depth and high temperatures, with possible involvement of mantle-derived magmas and followed by fractional crystallization, is increasingly accepted as the petrogenetic mechanism for generating A-type granites (e.g. Barbarin, 1999; Eby, 1992; Li et al., 2002). The whole-rock two-stage Nd model ages of the Azibailedi granites range from 2.26 to 2.38 Ga (Table 2), implying that the early Paleoproterozoic lower crust could be a potential source for the granites. Previous study on a mafic enclave occurring within

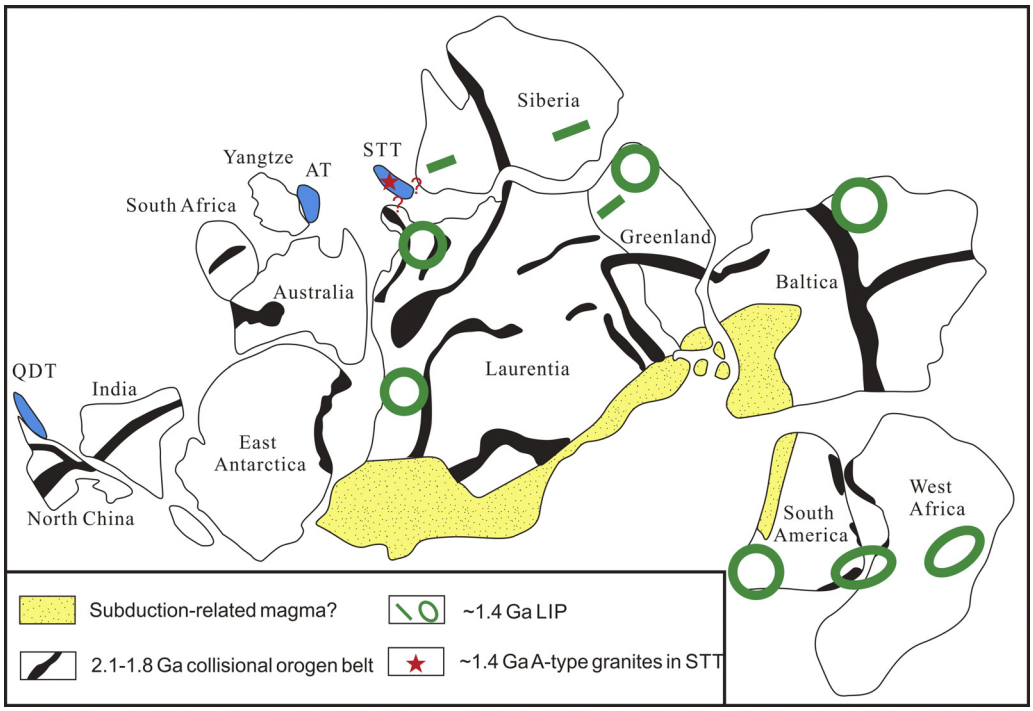

Fig. 13. Possible position of the STT in the Columbia supercontinent (modified after Zhao et al., 2002, 2004; Chen et al., 2013; Ernst et al., 2013; Zhang et al., 2014a).

the ~2.4 Ga granite yielded initial $\varepsilon_{Nd}(t)$ value of +2.15 at ~2.4 Ga (Zhang et al., 2007a) (Fig. 8), corresponding to $\varepsilon_{Nd}(t)$ value of −3.1 at ~1.4 Ga. The recalculated Nd isotopic composition falls within the range of $\varepsilon_{Nd}(t)$ values (−3.5 to −2.2) of the Azibailedi granites. Thus, the Nd isotope compositions suggest that the Azibailedi granitic pluton originated mainly from partial melting of the early Paleoproterozoic mafic lower crust.

However, the initial $\varepsilon_{Hf}(t)$ values of the Azibailedi granites vary between −4.1 and +6.1, suggesting the mixing of felsic magmas with variable amounts of basaltic magmas derived from depleted mantle sources. However, the granites have high zircon $\delta^{18}O$ values (7.1–8.7‰), which are obviously higher than those of zircons crystallized from the mantle-derived mafic magma. Thus, the possibility of incorporation of basaltic magmas could be excluded. The $\delta^{18}O$ values (7.1–8.7‰) are beyond the range of $\delta^{18}O$ values of 6.5–7.5‰ recognized for Archean TTG rocks (Valley et al., 2005), suggesting involvement of supracrustal components. On the other hand, zircons from the granites show few high positive initial $\varepsilon_{Hf}(t)$ values (+4.1 to +6.1), corresponding to relatively juvenile two-stage Hf model ages (1.93–2.11 Ga), arguing for the contribution of Paleoproterozoic juvenile crust.

Collectively, we propose that the magmas parental to the Azibailedi granites are alkaline felsic melts, which were most probably generated by partial melting of the pre-existing early Paleoproterozoic mafic lower crust with involvement of variable amount of Paleoproterozoic juvenile crust. The primitive magmas might have further experienced extensive differentiation, as inferred from the observed geochemical features of the Azibailedi granites.

6.3. Tectonic implications of the Azibailedi pluton

It is generally accepted that A-type granites are genetically related to extensional or non-compressional regimes and formed in both post-orogenic and/or anorogenic settings (Barbarin, 1999; Collins et al., 1982; Eby, 1992; Whalen et al., 1987, 1996).

Based on regional geology (see Section 2), there is no evidence for any Mesoproterozoic subduction-collision events in STT. Moreover, juvenile arc-related materials might have been involved in the genesis of the A-type granites which are genetically related to post-orogenic settings (e.g. Goodge and Vervoort, 2006). However, the high zircon $\delta^{18}O$ and weak positive $\varepsilon_{Hf}(t)$ values are in contrast with the involvement of juvenile materials. Accordingly, we conclude that the Azibailedi granites were formed in anorogenic setting rather than post-orogenic regime.

On the global-scale, ca. 1.4 Ga magmatic activities have been identified in many continental fragments, such as the 1410 Ma mafic dykes in both Fennoscandian Shield and Baltica Craton (Ernst and Buchan, 2001), the ~1.38 Ga mafic sills and their related volcanics in western Laurentia (western Canada and north-western America) (Abbott, 1997; Ernst and Buchan, 2001), the 1382 Ma Zig-Zag Dal basalts in northern Greenland (Upton et al., 2005), the 1384 mafic dyke swarms in northern Siberia (Ernst and Buchan, 2001), the ca. 1380 Ma Mashak igneous event in eastern Baltica (Puchkov et al., 2013), the 1380 Ma doleritic dykes in the West African Craton (El Bahat et al., 2013), the 1380–1370 Ma mafic-ultramafic complex and A-type granites in the southern margin of the Congo Craton (Ernst et al., 2013; Mayer et al., 2004) (Fig. 13).

We suggest that the formation of the Azibailedi A-type granite formed part of the global ca.1.4 Ga anorogenic igneous activity, most possibly related to the breakup of the Columbia supercontinent (Evans and Mitchell, 2011; Hou et al., 2008; Rogers and Santosh, 2002, 2009; Santosh, 2010; Santosh et al., 2006, 2009; Zhao et al., 2002, 2003, 2004, 2009, 2011; Zhang et al., 2009, 2012b; Meert, 2014).

6.4. Continental crust growth process of the STT

Granite is the main component of the continental crust on earth. Thus, the growth of the continental crust depends on the mode of generation of granitoid rocks (Wu et al., 2003; Castro, 2014). Conventionally, growth of juvenile continental crust is ascribed to occur at subduction zones or above mantle plumes. Particularly, the

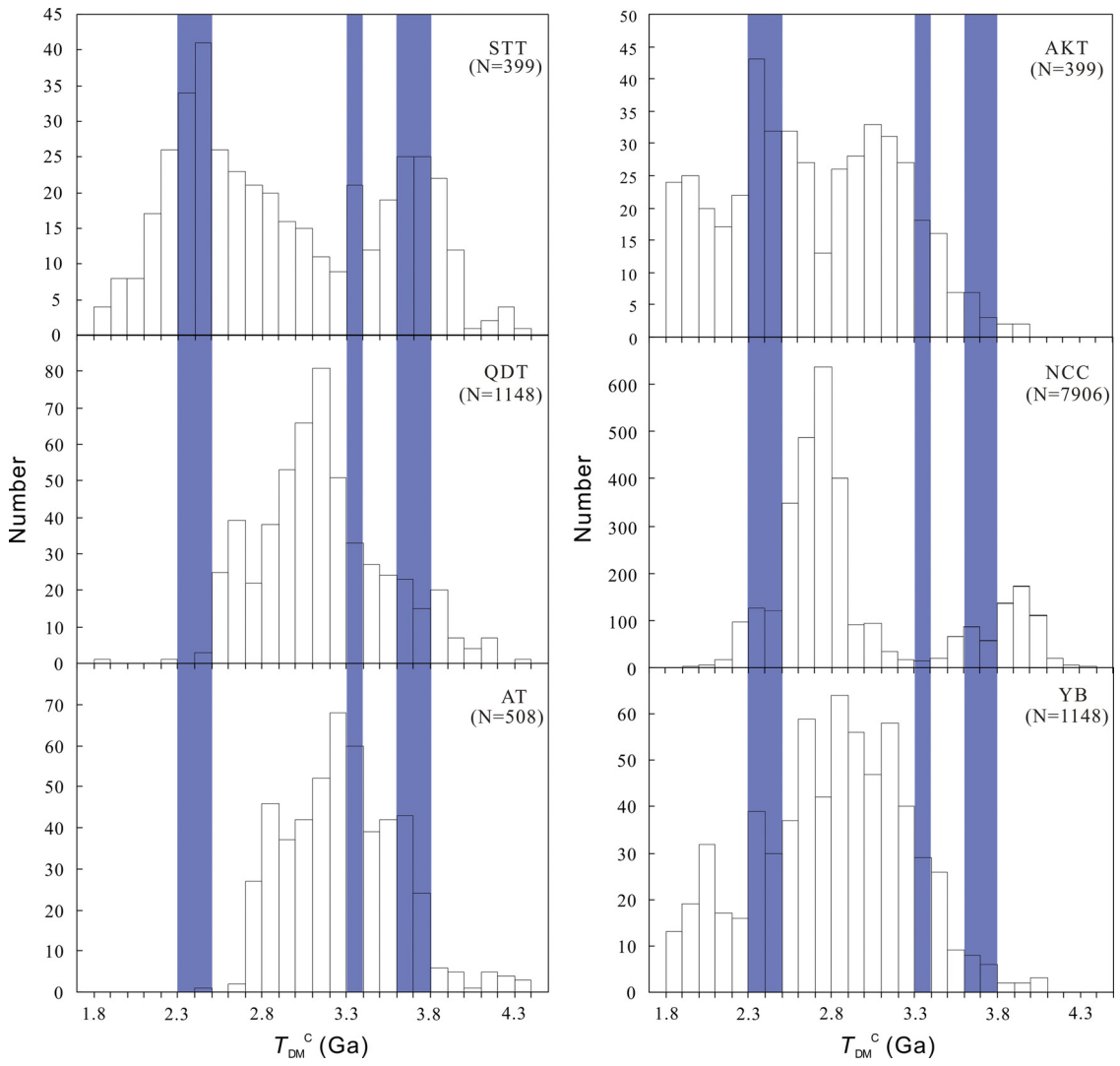

Fig. 14. Histograms of zircon Hf-crust model ages of early Precambrian rocks from STT, QDT, AT, AKT, NNC and YB. The data of the STT are from this study and our unpublished data; the data of the QDT are from Ge et al. (2013b, 2014), He et al. (2013), Long et al. (2010), and Zhang et al. (2013b); the data of the AT are from Long et al. (2014) and Zhang et al. (2014a); the data of NNC are from Geng et al. (2012) and Wan et al. (2015); the data of the YB are from Zhang et al. (2006a, b), Zhang and Zheng (2013), and Zhao et al. (2010). STT, Southwestern Tarim terrane; QDT, Quruqtagh-Dunhuang terrane; AT, Aketage terrane; AKT, Akesu terrane; NNC, North China Craton; YB, Yangtze Block.

former is the most important for the upper continental crust growth and the latter for the lower continental crust (Condie, 1997).

Compared with Sm–Nd isotope system, the Lu–Hf system is a better proxy to trace the evolution of continental crust (Hawkesworth and Kemp, 2006; Spencer et al., 2014; Lancaster et al., 2015). Moreover, zircon is a refractory mineral that forms a highly robust phase in most geological environments and thus is ideal for radiometric dating and geochemical tracing (e.g., Zheng et al., 2007). Thus, the zircon Hf isotope plays a pivotal role in unraveling the record of crustal evolution. In the STT, the distribution of Hf-crust model ages reveals that the early Precambrian continental crustal growth occurred mainly during 2.2–4.0 Ga, with major peaks at 2.3–2.5 Ga, 3.3 Ga and 3.6–3.8 Ga (Fig. 14).

In the Quruqtagh-Dunhuang terrane (QDT), crustal growth took place mainly during 2.5–3.9 Ga with major peaks at ca. 2.6–2.7 Ga and 3.0–3.2 Ga (Ge et al., 2013b, 2014; He et al., 2013; Long et al., 2010; Zhang et al., 2013b), which is similar to that of the North China Craton (NCC) (Geng et al., 2012 and references therein) (Fig. 14). In the Aketage terrane, zircon Hf isotope studies revealed that the growth of early Precambrian continental crust took place mainly during 2.7–3.8 Ga with peaks at 2.8 Ga, 3.3 Ga, 3.5–3.7 Ga (Long et al., 2014; Zhang et al., 2014a) which show significant affinity with that of Yangtze Block (YB) (Zhang et al., 2006a,b; Zhang and Zheng, 2013; Zhao et al., 2010) (Fig. 14). As for the Akesu terrane, the peaks of Hf-crustal model ages appear at 2.3–2.6 Ga and 3.0–3.2 Ga (Zhang et al., 2014b) (Fig. 14). The continental growth process of the individual terranes at different times from the Tarim Craton argue that the Precambrian basement of the Tarim was likely composed by discrete terranes detached from different Precambrian nuclei (Zhang et al., 2014a,b).

6.5. Possible affinity of the STT

Recently, Xu et al. (2013) classified the >900 Ma rocks in the Tarim Precambrian basement into three main tectonic units: the North Tarim terrane, the South Tarim terrane and the Neoproterozoic central suture zone. Nevertheless, according to the significant differences in timings of the late Paleoproterozoic collision events and the late Paleo-Mesoproterozoic breakup events among the different terranes of the Tarim Craton, Zhang et al. (2014a,b) proposed that the Precambrian basement of the Tarim Craton is composed of discrete terranes including Quruqtagh-Dunhuang terrane, Aketage terrane, Akesu terrane, southwest Tarim terrane and even some unknown terranes in central Tarim. Zhang et al. (2014a,b) argued

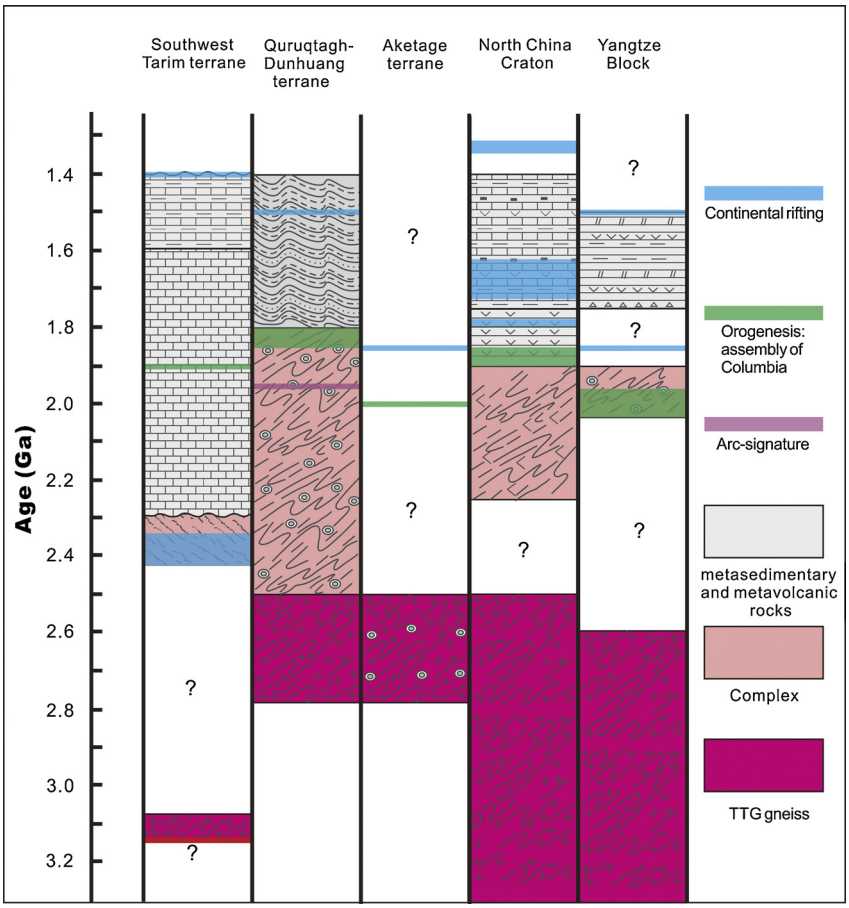

Fig. 15. Archean to Mesoproterozoic tectonothermal events of the STT, QDT, AT, YB and NNC. The data of the QDT are from Ge et al. (2013b), Lei et al. (2012), Wu et al. (2014), and Zhang et al. (2012a, 2013b); the data of the AT are from Long et al. (2014) and Zhang et al. (2014a); the data of the NNC are from Zhao and Zhai (2013) and Zhai et al. (2015); the data of the YB are from Chen et al. (2013) and references therein. The Precambrian rock series for the discrete terranes are from Zhai (2015). STT, Southwestern Tarim terrane; QDT, Quruqtagh-Dunhuang terrane; AT, Aketage terrane; NNC, North China Craton; YB, Yangtze Block.

that these terranes might have been derived from various continental nuclei.

Global-scale 2.1–1.8 Ga collision events have been well documented in a number of large continental cratons, and are linked with the assembly of the Columbia supercontinent (Rogers and Santosh, 2002, 2009; Santosh et al., 2006, 2009; Zhao et al., 2002, 2003, 2009, 2011; Meert, 2014). It is represented by the 2.1–2.0 Ga Transamazonian and Eburnean orogens in South America and West Africa; ~2.0 Ga Limpopo belt in south Africa and Capricorn Belt in Western Australia; 1.95–1.85 Ga Trans-Hudson Orogen or its equivalents in Laurentia (North America and Greenland); ~1.9 Ga Kola-Karelia, Volhyn-Central Russian, and Pachelma orogens in Baltica; and ~1.85 Ga Trans-North China Orogen in North China (Zhao et al., 2002, 2011; Yang and Santosh, 2015a,b).

The ~1.9 Ga metamorphism in the STT was believed to be related to the assembley of the Columbia supercontinent (Zhang et al., 2007a). Although no magmatic rocks of ~1.9 Ga have been reported in this terrane, the ~1.9 Ga detrital zircons of magmatic origin found in most of the volcano-sedimentary successions (Wang et al., 2015 and our unpublish data) are also indicative of this event.

In comparison with the timing of the Columbia supercontinent assembly, the STT is close to Laurentia, Siberia and Baltica (Fig. 13). Though at present it is difficult to correlate the STT with any of the three cratons above, it is obvious that the STT does not show any affinities with the Quruqtagh-Dunhuang or Aketage terrane, Akesu terranes (see Section 2). Furthermore, Zhang et al. (2014a,b) pointed out that the Quruqtagh-Dunhuang terrane shows clear affinity with that of the North China and the southern India Cratons (Figs. 13 and 15), whereas the Akesu terranes was possibly detached from the Yangtze-North Australia Craton (Figs. 13 and 15). Notably, the STT is different from both the North China Craton and Yangtze Block (Fig. 15).

In summary, the lack of synchronous nature in the late Paleoproterozoic orogenic events, as well as the differences in continental growth processes within the individual terranes of the Tarim Craton, we further confirm that the Precambrian basement of the Tarim Craton is composed of discrete terranes drifted from different Precambrian nuclei (e.g. Zhang et al., 2014a,b). Furthermore, these terranes had not amalgamated together until early Neoproterozoic during the assemblage of the Rodinia supercontinent.

7. Conclusions

The following conclusions can be drawn from this study.

(1) Zircon U–Pb dating indicates that the Azibailedi A-type granites in the STT were emplaced at ca. 1.4 Ga. The granites were most likely formed by partial melting of the pre-existing early Paleoproterozoic mafic lower crust with involvement of variable amounts of Paleoproterozoic juvenile crust, possibly from underplated basaltic magmas.
(2) The Azibailedi pluton was possibly related to the breakup of Columbia supercontinent. The STT might have been a fragment of the Paleo- to Mesoproterozoic Columbia supercontinent and was likely close to Laurentia Craton.

(3) Significant temporal discrepancy of Paleo- to Mesoproterozoic orogenic and extensional events and distinct timings in continental crustal growth processes for the different terranes in the Tarim Craton suggest that the basement of this craton was composed of discrete terranes during early Precambrian.

Acknowledgements

We appreciate the assistances of Hong-Ying Zhou in LA-ICP-MS dating, Qing-Xiu Meng and Qing-Bo Zhu in major element analyses by XRF, Liang Qi, Jing Hu and Wen-Jun Hu for trace element analyses by ICP-MS, Fang Xiao and Zhi-Bin Xiao for Sr–Nd isotope analyses by TIMS, Xiao-Xiao Ling and Guo-Qiang Tang for oxygen isotope analyses by SIMS. This study is financially supported by the National 305 Project of China (2015BAB05B01-02), National Science and Technology Major Project (2016ZX05004001-005) and National Science Foundation of China (41172175).

Appendix A. Supplementary data

Supplementary data associated with this article can be found, in the online version, at http://dx.doi.org/10.1016/j.precamres.2015.12.017.

References

Abbott, J.G., 1997. Geology of the upper Hart River area, eastern Ogilvie Mountains, Yukon Territory (116A/10, 116A/11). Exploration and Geological Services Division, Yukon Region, Indian and Northern Affairs Canada, Bulletin 9.
Anderson, I.C., Frost, C.D., Frost, B.R., 2003. Petrogenesis of the Red Mountain pluton, Laramie anorthosite complex, Wyoming: implications for the origin of A-type granite. Precambrian Res. 124, 243–267.
Barbarin, B., 1999. A review of the relationships between granitoid types, their origins and their geodynamic environments. Lithos 46, 605–626.
Bonin, B., 2007. A-type granites and related rocks: evolution of a concept, problems and prospects. Lithos 97, 1–29.
Boynton, W.V., 1984. Geochemistry of the rare earth elements: meteorite studies. In: Henderson, P. (Ed.), Rare Earth Element Geochemistry. Elsevier, pp. 63–114.
Castro, A., 2014. The off-crust origin of granite batholiths. Geosci. Front. 5, 73–75.
Chen, W.T., Zhou, M.-F., Zhao, X.-F., 2013. Late Paleoproterozoic sedimentary and mafic rocks in the Hekou area, SW China: implication for the reconstruction of the Yangtze Block in Columbia. Precambrian Res. 231, 61–77.
Collins, W.J., Beams, S.D., White, A.J.R., Chappell, B.W., 1982. Nature and origin of A-type granites with particular reference to southeastern Australia. Contrib. Mineral. Petrol. 80, 189–200.
Condie, K.C., 1997. Contrasting sources for upper and lower continental crust: the greenstone connection. J. Geol. 105, 729–736.
Dall'Agnol, R., de Oliveira, D.C., 2007. Oxidized, magnetite-series, rapakivi-type granites of Carajás, Brazil: implications for classification and petrogenesis of A-type granites. Lithos 93, 215–233.
Eby, G.N., 1990. The A-type granitoids-a review of their occurrence and chemical characteristics and speculations on their petrogenesis. Lithos 26, 115–134.
Eby, G.N., 1992. Chemical subdivision of the A-type granitoids-petrogenetic and tectonic implications. Geology 20, 641–644.
El Bahat, A., Ikenne, M., Söderlund, U., Cousens, B., Youbi, N., Ernst, R., Soulaimani, A., Hafid, A., 2013. U–Pb baddeleyite ages and geochemistry of dolerite dykes in the Bas Drâa Inlier of the Anti-Atlas of Morocco: newly identified 1380 Ma event in the West African Craton. Lithos 174, 85–98.
Ernst, R.E., Buchan, K.L., 2001. Large mafic magmatic events through time and links to mantle-plume heads. In: Ernst, R.E., Buchan, K.L. (Eds.), Geological Society of America Special Paper. , pp. 483–576.
Ernst, R.E., Pereira, E., Hamilton, M.A., Pisarevsky, S.A., Rodriques, J., Tassinari, C.C., Teixeira, W., Van-Dunem, V., 2013. Mesoproterozoic intraplate magmatic 'barcode' record of the Angola portion of the Congo Craton: newly dated magmatic events at 1505 and 1110 Ma and implications for Nuna (Columbia) supercontinent reconstructions. Precambrian Res. 230, 103–118.
Evans, D.A., Mitchell, R.N., 2011. Assembly and breakup of the core of Paleoproterozoic–Mesoproterozoic supercontinent Nuna. Geology 39, 443–446.
Feng, B.Z., Zhou, Y.W., Chi, S.F., Yang, T.Q., Zhong, C.X., Ye, S.Q., 1995. Pre-Sinian Geology and Noble Metals, Colored Metals Mineralization in Quruqtagh, Xinjiang. Geological Publishing House, Beijing, pp. 1–282 (in Chinese with English abstract).
Frost, B.R., Barnes, C.G., Collins, W.J., Arculus, R.J., Ellis, D.J., Frost, C.D., 2001. A geochemical classification for granitic rocks. J. Petrol. 42, 2033–2048.
Frost, B.R., Frost, C.D., 2008. A geochemical classification for feldspathic igneous rocks. J. Petrol. 49, 1955–1969.
Ge, R.F., Zhu, W.B., Wu, H.L., He, J.W., Zheng, B., 2013a. Zircon U–Pb ages and Lu–Hf isotopes of Paleoproterozoic metasedimentary rocks in the Korla Complex, NW China: implications for metamorphic zircon formation and geological evolution of the Tarim Craton. Precambrian Res. 231, 1–18.
Ge, R.F., Zhu, W.B., Wilde, S.A., He, J.W., 2014. Zircon U–Pb–Lu–Hf–O isotopic evidence for ≥3.5 Ga crustal growth, reworking and differentiation in the northern Tarim Craton. Precambrian Res. 249, 115–128.
Ge, R.F., Zhu, W.B., Wu, L., Zheng, B.H., He, J.W., 2013b. Timing and mechanisms of multiple episodes of migmatization in the Korla Complex, northern Tarim Craton, NW China: constraints from zircon U–Pb–Lu–Hf isotopes and implications for crustal growth. Precambrian Res. 231, 136–156.
Geng, J.Z., Li, H.K., Zhang, J., Zhang, Y.Q., 2011. Zircon Hf isotope analysis by means of LA-MC-ICP-MS. Geol. Bull. China 30, 1508–1513 (in Chinese with English abstract).
Geng, Y.S., Du, L.L., Ren, L.D., 2012. Growth and reworking of the early Precambrian continental crust in the North China Craton: constraints from zircon Hf isotopes. Gondwana Res. 21, 517–529.
Goodge, J.W., Vervoort, J.D., 2006. Origin of Mesoproterozoic A-type granites in Laurentia: Hf isotope evidence. Earth Planet. Sci. Lett. 243, 711–731.
Guo, X.C., Zheng, Y.Z., Gao, J., Zhu, Z.X., 2013. Determination and geological significance of the Mesoarchean Craton in Western Kunlun Mountains, Xinjiang, China. Geol. Rev. 59, 401–412.
Han, B.F., Wang, S.G., Jahn, B.M., Hong, D.W., Kagami, H., Sun, Y.L., 1997. Depleted-mantle source for the Ulungur River A-type granites from North Xinjiang, China: geochemistry and Nd–Sr isotopic evidence, and implications for Phanerozoic crustal growth. Chem. Geol. 138, 135–159.
Hawkesworth, C.J., Kemp, A.I.S., 2006. Using hafnium and oxygen isotopes in zircons to unravel the record of crustal evolution. Chem. Geol. 226, 144–162.
He, Z.Y., Sun, L.X., Mao, L.J., Zong, K.Q., Zhang, Z.M., 2015a. Zircon U–Pb and Hf isotopic study of gneiss and granodiorite from the southern Beishan orogenic collage: Mesoproterozoic magmatism and crustal growth. Chin. Sci. Bull. 60 (Chinese version).
He, Z.Y., Zhang, Z.M., Zong, K.Q., Dong, X., 2013. Paleoproterozoic crustal evolution of the Tarim Craton: constrained by zircon U–Pb and Hf isotopes of meta-igneous rocks from Korla and Dunhuang. J. Asian Earth Sci. 78, 54–70.
He, X.F., Santosh, M., Tsunogae, T., Malaviarachchi, S.P.K., 2015b. Early to late Neoproterozoic magmatism and magma mixing-mingling in Sri Lanka: implications for convergent margin processes during Gondwana assembly. Gondwana Res., http://dx.doi.org/10.1016/j.gr.2015.02.013.
Heilimo, E., Elburg, M.A., Andersen, T., 2014. Crustal growth and reworking during Lapland–Kola orogeny in northern Fennoscandia: U–Pb and Lu–Hf data from the Nattanen and Litsa–Aragub-type granites. Lithos 205, 112–126.
HNGS, 2004a. Geological Map of Taxkorgan County, Xinjiang, China, Scale 1: 250000. Henan Institute of Geological Survey (in Chinese).
HNGS, 2004b. Geological Map of Yecheng County, Xinjiang, China, Scale 1: 250000. Henan Institute of Geological Survey (in Chinese).
Hou, G.T., Santosh, M., Qian, X.L., Lister, G.S., Li, J.H., 2008. Tectonic constraints on 1.3 similar to 1.2 Ga final breakup of Columbia supercontinent from a giant radiating dyke swarm. Gondwana Res. 14, 561–566.
Hou, K.J., Li, Y.H., Tian, Y.R., 2009. In situ U–Pb zircon dating using laser ablation-multi ion counting ICP-MS. Miner. Depos. 28, 481–492 (in Chinese with English abstract).
Hu, A.Q., Jahn, B.M., Zhang, G.X., Chen, Y.B., Zhang, Q.F., 2000. Crustal evolution and Phanerozoic crustal growth in northern Xinjiang: Nd isotopic evidence. Part I. Isotopic characterization of basement rocks. Tectonophysics 328, 15–51.
Huang, J.G., Yang, R.D., Yang, J., Cui, C.L., Hou, L.J., 2012. Mesoproterozoic magmatic activities and its geological significance in Kusilafu area of the northern margin of western Kunlun. Chin. J. Geol. 47, 867–885.
Huang, X.-L., Xu, Y.-G., Li, X.-H., Li, W.-X., Lan, J.-B., Zhang, H.-H., Liu, Y.-S., Wang, Y.-B., Li, H.-Y., Luo, Z.-Y., Yang, Q.-J., 2008. Petrogenesis and tectonic implications of Neoproterozoic, highly fractionated A-type granites from Mianning, South China. Precambrian Res. 165, 190–204.
Jahn, B.M., 2004. The central Asian orogenic belt and growth of the continental crust in the phanerozoic. Geol. Soc. Lond. Spec. Publ. 226, 73–100.
Jahn, B.M., Wu, F.Y., Lo, C.H., Tsai, C.H., 1999. Crust–mantle interaction induced by deep subduction of the continental crust: geochemical and Sr–Nd isotopic evidence from post-collisional mafic–ultramafic intrusions of the northern Dabie complex, central China. Chem. Geol. 157, 119–146.
Jung, S., Hoernes, S., Mezger, K., 2000. Geochronology and petrogenesis of Pan-African, syn-tectonic, S-type and post-tectonic A-type granite (Namibia): products of melting of crustal sources, fractional crystallization and wall rock entrainment. Lithos 50, 259–287.
Jung, S., Mezger, K., Hoernes, S., 1998. Petrology and geochemistry of syn- to post-collisional metaluminous A-type granites – a major and trace element and Nd–Sr–Pb–O-isotope study from the Proterozoic Damara Belt, Namibia. Lithos 45, 147–175.
King, P.L., White, A.J.R., Chappell, B.W., Allen, C.M., 1997. Characterization and origin of aluminous A-type granites from the Lachlan Fold Belt, Southeastern Australia. J. Petrol. 38, 371–391.
Lancaster, P.J., Dey, S., Storey, C.D., Mitra, A., Bhunia, R.K., 2015. Contrasting crustal evolution processes in the Dharwar craton: insights from detrital zircon U–Pb and Hf isotopes. Gondwana Res. 28, 1361–1372.
Lei, R., Wu, C., Chi, G., Chen, G., Gu, L., Jiang, Y., 2012. Petrogenesis of the Palaeoproterozoic Xishankou pluton, northern Tarim block, northwest China: implications for assembly of the supercontinent Columbia. Int. Geol. Rev. 54, 1829–1842.
Li, X.H., Li, W.X., Li, Q.L., Wang, X.C., Liu, Y., Yang, Y.H., 2010a. Petrogenesis and tectonic significance of the ~850 Ma Gangbian alkaline complex in South China:

evidence from in situ zircon U–Pb dating, Hf–O isotopes and whole-rock geochemistry. Lithos 114, 1–15.
Li, X.H., Li, Z.X., Zhou, H., Liu, Y., Kinny, P.D., 2002. U–Pb zircon geochronology, geochemistry and Nd isotopic study of Neoproterozoic bimodal volcanic rocks in the Kangdian Rift of South China: implications for the initial rifting of Rodinia. Precambrian Res. 113, 135–154.
Li, X.H., Liu, D.Y., Sun, M., Li, W.X., Liang, X.R., Liu, Y., 2004. Precise Sm–Nd and U–Pb isotopic dating of the super-giant Shizhuyuan polymetallic deposit and its host granite; Southeast China. Geol. Mag. 141, 225–231.
Li, X.H., Long, W.G., Li, Q.L., Liu, Y., Zheng, Y.F., Yang, Y.H., Chamberlain, K.R., Wan, D.F., Guo, C.H., Wang, X.C., 2010b. Penglai zircon megacrysts: a potential new working reference material for microbeam determination of Hf–O isotopes and U–Pb age. Geostand. Geoanal. Res. 34, 117–134.
Li, X.H., Tang, G.Q., Gong, B., Yang, Y.H., Hou, K.J., Hu, Z.C., Li, Q.L., Liu, Y., Li, W.X., 2013. Qinghu zircon: a working reference for microbeam analysis of U–Pb age and Hf and O isotopes. Chin. Sci. Bull. 58, 4647–4654.
Liu, Y.S., Gao, S., Hu, Z.C., Gao, C.G., Zong, K.Q., Wang, D.B., 2009. Continental and oceanic crust recycling-induced melt–peridotite interactions in the Trans-North China Orogen: U–Pb dating, Hf isotopes and trace elements in zircons from mantle xenoliths. J. Petrol. 51, 537–571.
Liu, Y.S., Hu, Z.C., Zong, K.Q., Gao, C.G., Gao, S., Xu, J., Chen, H.H., 2010. Reappraisement and refinement of zircon U–Pb isotope and trace element analyses by LA-ICP-MS. Chin. Sci. Bull. 55, 1535–1546.
Loiselle, M.C., Wones, D.R., 1979. Characteristics and origin of anorogenic granites. Geol. Soc. Am. Abstr. Progr. 11, 468.
Long, X.P., Yuan, C., Sun, M., Kröner, A., Zhao, G.C., 2014. New geochemical and combined zircon U–Pb and Lu–Hf isotopic data of orthogneisses in the northern Altyn Tagh, northern margin of the Tibetan plateau: implication for Archean evolution of the Dunhuang Block and crust formation in NW China. Lithos 200–201, 418–431.
Long, X.P., Yuan, C., Sun, M., Zhao, G.C., Xiao, W.J., Wang, Y.J., Yang, Y.H., Hu, A.Q., 2010. Archean crustal evolution of the northern Tarim craton, NW China: zircon U–Pb and Hf isotopic constraints. Precambrian Res. 180, 272–284.
Lu, S.N., Li, H.K., Zhang, C.L., Niu, G.H., 2008. Geological and geochronological evidence for the Precambrian evolution of the Tarim Craton and surrounding continental fragments. Precambrian Res. 160, 94–107.
Ludwig, K.R., 1999. Using Isoplot/EX, Version 2, A Geolocronolgical Toolkit for Microsoft Excel, vol. 1a. Berkeley Geochronological Center Special Publication, pp. 47.
Lugmair, G.W., Harti, K., 1978. Lunar initial $^{143}Nd/^{144}Nd$: differential evolution of the lunar crust and mantle. Earth Planet. Sci. Lett. 39, 349–357.
Maniar, P.D., Piccoli, P.M., 1989. Tectonic discrimination of granitoids. Geol. Soc. Am. Bull. 101, 635–643.
Mayer, A., Hofmann, A., Sinigoi, S., Morais, E., 2004. Mesoproterozoic Sm–Nd and U–Pb ages for the Kunene anorthosite complex of SW Angola. Precambrian Res. 133, 187–206.
Meert, J.G., 2014. Strange attractors, spiritual interlopers and lonely wanderers: the search for pre-Pangean supercontinents. Geosci. Front. 5, 155–166.
Miller, C.F., McDowell, S.M., Mapes, R.W., 2003. Hot and cold granites? Implications of zircon saturation temperatures and preservation of inheritance. Geology 31, 529–532.
Puchkov, V.N., Bogdanova, S.V., Ernst, R.E., Kozlov, V.I., Krasnobaev, A.A., Söderlund, U., Wingate, M.T., Postnikov, A.V., Sergeeva, N.D., 2013. The ca. 1380 Ma Mashak igneous event of the Southern Urals. Lithos 174, 109–124.
Qi, L., Hu, J., Gregoire, D.C., 2000. Determination of trace elements in granites by inductively coupled plasma mass spectrometry. Talanta 51, 507–513.
Renjith, M.L., Charan, S.N., Subbarao, D.V., Babu, E.V.S.S.K., Rajashekhar, V.B., 2014. Grain to outcrop-scale frozen moments of dynamic magma mixing in the syenite magma chamber, Yelagiri Alkaline Complex, South India. Geosci. Front. 5, 801–820.
Rogers, J.J.W., Santosh, M., 2002. Configuration of Columbia, a mesoproterozoic supercontinent. Gondwana Res. 5, 5–22.
Rogers, J.J.W., Santosh, M., 2009. Tectonics and surface effects of the supercontinent Columbia. Gondwana Res. 15, 373–380.
Rudnick, R.L., Gao, S., 2003. Composition of the continental crust. In: Holland, H.D., Turekin, K.K. (Eds.), Treatise on Geochemistry. Elsevier, pp. 1–64.
Santosh, M., 2010. Assembling North China Craton within the Columbia supercontinent: the role of double-sided subduction. Precambrian Res. 178, 149–167.
Santosh, M., Sajeev, K., Li, J.H., 2006. Extreme crustal metamorphism during Columbia supercontinent assembly: evidence from North China Craton. Gondwana Res. 10, 256–266.
Santosh, M., Wan, Y.S., Liu, D.Y., Chunyan, D., Li, J.H., 2009. Anatomy of zircons from an ultrahot Orogen: the amalgamation of the North China Craton within the Supercontinent Columbia. J. Geol. 117, 429–443.
Spencer, C.J., Cawood, P.A., Hawkesworth, C.J., Prave, A.R., Roberts, N.M.W., Horstwood, M.S.A., Whitehouse, M.J., ElMF, 2014. Generation and preservation of continental crust in the Grenville Orogeny. Geosci. Front. 6, 357–362, http://dx.doi.org/10.1016/j.gsf.2014.12.001.
Sun, S.-S., McDonough, W.F., 1989. Chemical and isotopic systematics of ocean basalts: implications for mantle composition and process. In: Saunders, A.D., Norry, M.J. (Eds.), Magmatism in the Ocean Basins. Geological Society. Special Publications, London, pp. 313–345.
Upton, B., Rämö, O., Heaman, L., Blichert-Toft, J., Kalsbeek, F., Barry, T., Jepsen, H., 2005. The Mesoproterozoic Zig-Zag Dal basalts and associated intrusions of eastern North Greenland: mantle plume–lithosphere interaction. Contrib. Mineral. Petrol. 149, 40–56.
Valley, J., Lackey, J., Cavosie, A., Clechenko, C., Spicuzza, M., Basei, M., Bindeman, I., Ferreira, V., Sial, A., King, E., 2005. 4.4 billion years of crustal maturation: oxygen isotope ratios of magmatic zircon. Contrib. Mineral. Petrol. 150, 561–580.
Valley, J.W., Kinny, P.D., Schulze, D.J., Spicuzza, M.J., 1998. Zircon megacrysts from kimberlite: oxygen isotope variability among mantle melts. Contrib. Mineral. Petrol. 133, 1–11.
Wan, Y.-S., Liu, D.-Y., Dong, C.-Y., Xie, H.-Q., Kröner, A., Ma, M.-Z., Liu, S.-J., Xie, S.-W., Ren, P., 2015. Formation and Evolution of Archean Continental Crust of the North China Craton, Precambrian Geology of China. Springer, pp. 59–136.
Wang, C., Wang, Y.H., Liu, L., He, S.P., Li, R.S., Li, M., Yang, W.Q., Cao, Y.-T., Meert, J.G., Shi, C., 2014. The Paleoproterozoic magmatic–metamorphic events and cover sediments of the Tiekelik Belt and their tectonic implications for the southern margin of the Tarim Craton, northwestern China. Precambrian Res. 254, 210–225.
Wang, C., Liu, L., Wang, Y.H., He, S.P., Li, R.S., Li, M., Yang, W.Q., Cao, Y.T., Collins, A.S., Shi, C., Wu, Z.N., 2015. Recognition and tectonic implications of an extensive Neoproterozoic volcano-sedimentary rift basin along the southwestern margin of the Tarim Craton, northwestern China. Precambrian Res. 257, 65–82.
Wang, Q., Wyman, D.A., Li, Z.-X., Bao, Z.-W., Zhao, Z.-H., Wang, Y.-X., Jian, P., Yang, Y.-H., Chen, L.-L., 2010. Petrology, geochronology and geochemistry of ca. 780 Ma A-type granites in South China: petrogenesis and implications for crustal growth during the breakup of the supercontinent Rodinia. Precambrian Res. 178, 185–208.
Watson, E.B., Harrison, T.M., 1983. Zircon saturation revisited: temperature and composition effects in a variety of crustal magma types. Earth Planet. Sci. Lett. 64, 295–304.
Whalen, J.B., Currie, K.L., Chappell, B.W., 1987. A-type granites-geochemical characteristics, discrimination and petrogenesis. Contrib. Mineral. Petrol. 95, 407–419.
Whalen, J.B., Jenner, G.A., Longstaffe, F.J., Robert, F., Gariepy, C., 1996. Geochemical and isotopic (O, Nd, Pb and Sr) constraints on a type granite petrogenesis based on the topsails igneous suite, Newfoundland Appalachians. J. Petrol. 37, 1463–1489.
Wu, C.Z., Santosh, M., Chen, Y.J., Samson, I.M., Lei, R.X., Dong, L.H., Qu, X., Gu, L.X., 2014. Geochronology and geochemistry of Early Mesoproterozoic meta-diabase sills from Quruqtagh in the northeastern Tarim Craton: implications for breakup of the Columbia supercontinent. Precambrian Res. 241, 29–43.
Wu, F.Y., Jahn, B.M., Wilde, S.A., Lo, C.H., Yui, T.F., Lin, Q., Ge, W.C., Sun, D.Y., 2003. Highly fractionated I-type granites in NE China (II): isotopic geochemistry and implications for crustal growth in the Phanerozoic. Lithos 67, 191–204.
Wu, F.Y., Sun, D.Y., Li, H.M., Jahn, B.M., Wilde, S., 2002. A-type granites in northeastern China: age and geochemical constraints on their petrogenesis. Chem. Geol. 187, 143–173.
Wu, F.Y., Yang, Y.H., Xie, L.W., Yang, J.H., Xu, P., 2006. Hf isotopic compositions of the standard zircons and baddeleyites used in U–Pb geochronology. Chem. Geol. 234, 105–126.
Xinjiang Bureau of Geology and Mineral Resources, 1993. Lithotratigraphy of Xinjiang Uygur Autonomous Region. China University of Geology Publishing House, Wuhan, pp. 5–57 (in Chinese).
Xu, Z.Q., He, B.Z., Zhang, C.L., Zhang, J.X., Wang, Z.M., Cai, Z.H., 2013. Tectonic framework and crustal evolution of the Precambrian basement of the Tarim Block in NW China: new geochronological evidence from deep drilling samples. Precambrian Res. 235, 150–162.
Yang, J.H., Wu, F.Y., Chung, S.L., Wilde, S.A., Chu, M.F., 2006. A hybrid origin for the Qianshan A-type granite, northeast China: geochemical and Sr–Nd–Hf isotopic evidence. Lithos 89, 89–106.
Yang, Q.Y., Santosh, M., 2015a. Paleoproterozoic arc magmatism in the North China Craton: no Siderian global plate tectonic shutdown. Gondwana Res. 28, 82–105, http://dx.doi.org/10.1016/j.gr.2014.08.005.
Yang, Q.Y., Santosh, M., 2015b. Charnockite magmatism during a transitional phase: implications for Late Paleoproterozoic ridge subduction in the North China Craton. Precambrian Res., http://dx.doi.org/10.1016/j.precamres.2015.01.014.
Yong, W., Zhang, L., Hall, C., Mukasa, S., Essene, E., 2013. The $^{40}Ar/^{39}Ar$ and Rb–Sr chronology of the Precambrian Aksu blueschists in western China. J. Asian Earth Sci. 63, 197–205.
Zhai, M.G., 2015. Precambrian Geology of China. Springer, pp. 1–390.
Zhai, M.G., Hu, B., Zhao, T.P., Peng, P., Meng, Q.R., 2015. Late Paleoproterozoic–Neoproterozoic multi-rifting events in the North China Craton and their geological significance: a study advance and review. Tectonophysics, http://dx.doi.org/10.1016/j.tecto.2015.01.019.
Zhang, C.L., Li, H.K., Santosh, M., Li, Z.X., Zou, H.B., Wang, H.Y., Ye, H.M., 2012a. Precambrian evolution and cratonization of the Tarim Block, NW China: petrology, geochemistry, Nd-isotopes and U–Pb zircon geochronology from Archaean gabbro-TTG-potassic granite suite and Paleoproterozoic metamorphic belt. J. Asian Earth Sci. 47, 5–20.
Zhang, C.L., Li, Z.X., Li, X.H., Ye, H.M., Wang, A.G., Guo, K.Y., 2006a. Neoproterozoic bimodal intrusive complex in the southwestern Tarim Block, Northwest China: age, geochemistry, and implications for the rifting of Rodinia. Int. Geol. Rev. 48, 112–128.
Zhang, C.L., Li, Z.X., Li, X.H., Yu, H.F., Ye, H.M., 2007a. An early Paleoproterozoic high-K intrusive complex in southwestern Tarim block, NW China: age, geochemistry, and tectonic implications. Gondwana Res. 12, 101–112.
Zhang, C.L., Lu, S.N., Yu, H.F., Ye, H.M., 2007b. Tectonic evolution of the Western Kunlun orogenic belt in northern Qinghai-Tibet Plateau: evidence from zircon SHRIMP and LA-ICP-MS U–Pb geochronology. Sci. China Ser. D: Earth Sci. 50, 825–835.

Zhang, C.L., Wang, Z.G., Shen, J.L., Bi, H., Guo, K.Y., Wang, A.G., 2003. Zircon SHRIMP dating and geochemistry characteristics of Akazi rock mass of Western Kunlun. Acta Petrol. Sin. 19, 523–529.
Zhang, C.L., Yang, D.S., Wang, H.Y., Dong, Y.G., Ye, H.M., 2010. Neoproterozoic Mafic Dykes and Basalts in the Southern Margin of Tarim, Northwest China: age, geochemistry and geodynamic implications. Acta Geol. Sin. Engl. Ed. 84, 549–562.
Zhang, C.L., Ye, H.M., Wang, A.G., Guo, K.Y., Dong, Y.G., 2004. Geochemistry of the Neoproterozoic diabase and basalt in South of Tarim plate: evidence for the Neoproterozoic breakup of the Rodinia super-continent in south of Tarim. Acta Petrol. Sin. 20, 473–482.
Zhang, C.L., Zou, H.B., 2013. Permian A-type granites in Tarim and western part of Central Asian Orogenic Belt (CAOB): genetically related to a common Permian mantle plume? Lithos 172–173, 47–60.
Zhang, C.L., Zou, H.B., Li, H.K., Wang, H.Y., 2013a. Tectonic framework and evolution of the Tarim Block in NW China. Gondwana Res. 23, 1306–1315.
Zhang, C.L., Zou, H.B., Santosh, M., Ye, X.T., Li, H.K., 2014a. Is the Precambrian basement of the Tarim Craton in NW China composed of discrete terranes? Precambrian Res. 254, 226–244.
Zhang, J., Zhang, C.L., Li, H.K., Ye, X.T., Geng, J.Z., Zhou, H.Y., 2014b. Revisit to time and tectonic environment of the Akesu blueschist terrane in northern Tarim, NW China: new evidence from zircon U–Pb age and Hf isotope. Acta Petrol. Sin. 30, 3357–3365.
Zhang, J.X., Yu, S.Y., Gong, J.H., Li, H.K., Hou, K.J., 2013b. The latest Neoarchean-Paleoproterozoic evolution of the Dunhuang block, eastern Tarim craton, northwestern China: evidence from zircon U–Pb dating and Hf isotopic analyses. Precambrian Res. 226, 21–42.
Zhang, S.B., Zheng, Y.F., 2013. Formation and evolution of Precambrian continental lithosphere in South China. Gondwana Res. 23, 1241–1260.
Zhang, S.B., Zheng, Y.F., Wu, Y.B., Zhao, Z.F., Gao, S., Wu, F.Y., 2006b. Zircon U–Pb age and Hf isotope evidence for 3.8 Ga crustal remnant and episodic reworking of Archean crust in South China. Earth Planet. Sci. Lett. 252, 56–71.
Zhang, S.H., Li, Z.X., Evans, D.A.D., Wu, H.C., Li, H.Y., Dong, J., 2012b. Pre-Rodinia supercontinent Nuna shaping up: a global synthesis with new paleomagnetic results from North China. Earth Planet. Sci. Lett. 353–354, 145–155.
Zhang, S.H., Zhao, Y., Yang, Z.Y., He, Z.F., Wu, H., 2009. The 1.35 Ga diabase sills from the northern North China Craton: implications for breakup of the Columbia (Nuna) supercontinent. Earth Planet. Sci. Lett. 288, 588–600.
Zhao, G.C., Cawood, P.A., 2012. Precambrian geology of China. Precambrian Res. 222, 13–54.
Zhao, G.C., Cawood, P.A., Wilde, S.A., Sun, M., 2002. Review of global 2.1–1.8 Ga orogens: implications for a pre-Rodinia supercontinent. Earth-Sci. Rev. 59, 125–162.
Zhao, G.C., He, Y.H., Sun, M., 2009. The Xiong'er volcanic belt at the southern margin of the North China Craton: petrographic and geochemical evidence for its outboard position in the Paleo-Mesoproterozoic Columbia Supercontinent. Gondwana Res. 16, 170–181.
Zhao, G.C., Li, S.Z., Sun, M., Wilde, S.A., 2011. Assembly, accretion, and break-up of the Palaeo-Mesoproterozoic Columbia supercontinent: record in the North China Craton revisited. Int. Geol. Rev. 53, 1331–1356.
Zhao, G.C., Sun, M., Wilde, S.A., Li, S.Z., 2003. Assembly, accretion and breakup of the paleo-mesoproterozoic Columbia supercontinent: records in the North China Craton. Gondwana Res. 6, 417–434.
Zhao, G.C., Sun, M., Wilde, S.A., Li, S.Z., 2004. A Paleo-Mesoproterozoic supercontinent: assembly, growth and breakup. Earth-Sci. Rev. 67, 91–123.
Zhao, G.C., Zhai, M.G., 2013. Lithotectonic elements of Precambrian basement in the North China Craton: review and tectonic implications. Gondwana Res. 23, 1207–1240.
Zhao, X.F., Zhou, M.F., Li, J.W., Sun, M., Gao, J.F., Sun, W.H., Yang, J.H., 2010. Late Paleoproterozoic to early Mesoproterozoic Dongchuan Group in Yunnan, SW China: implications for tectonic evolution of the Yangtze Block. Precambrian Res. 182, 57–69.
Zhao, X.F., Zhou, M.F., Li, J.W., Wu, F.Y., 2008. Association of Neoproterozoic A- and I-type granites in South China: implications for generation of A-type granites in a subduction-related environment. Chem. Geol. 257, 1–15.
Zheng, Y.F., Zhang, S.B., Zhao, Z.F., Wu, Y.B., Li, X.H., Li, Z.X., Wu, F.Y., 2007. Contrasting zircon Hf and O isotopes in the two episodes of Neoproterozoic granitoids in South China: implications for growth and reworking of continental crust. Lithos 96, 127–150.
Zhong, H., Zhu, W.-G., Chu, Z.-Y., He, D.-F., Song, X.-Y., 2007. SHRIMP U–Pb zircon geochronology, geochemistry, and Nd–Sr isotopic study of contrasting granites in the Emeishan large igneous province, SW China. Chem. Geol. 236, 112–133.
Zhu, W., Zheng, B., Shu, L., Ma, D., Wu, H., Li, Y., Huang, W., Yu, J., 2011. Neoproterozoic tectonic evolution of the Precambrian Aksu blueschist terrane, northwestern Tarim, China: insights from LA-ICP-MS zircon U–Pb ages and geochemical data. Precambrian Res. 185, 215–230.
Zhu, W.G., Zhong, H., Li, X.H., He, D.F., Song, X.Y., Ren, T., Chen, Z.Q., Sun, H.S., Liao, J.Q., 2010. The early Jurassic mafic-ultramafic intrusion and A-type granite from northeastern Guangdong, SE China: age, origin, and tectonic significance. Lithos 119, 313–329.